Preprints.org

Article

Investigation on the Mechanical Characteristics of Excavation of Double-Line Highway Tunnel Underpass Existing Railway Tunnel under the Influence of Dynamic and Static Load

Yifan Li , Changfu Huang , Hongjian Lu [*] , Chao Mou [*]

Article

Investigation on the Mechanical Characteristics of Excavation of Double-Line Highway Tunnel Underpass Existing Railway Tunnel under the Influence of Dynamic and Static Load

Yifan Li [1], Changfu Huang [1], Hongjian Lu [2],* and Chao Mou [2],*

[1] School of Civil and Environment Engineering, University of Science and Technology Beijing, Beijing 100083,C-hina; b20160022@xs.ustb.edu.cn(Y.L.); hchf@ sohu.com(C.H.)

[2] Shool of Mine Engineering, North China University of Science and Technology, Tangshan 063210,China

* Correspondence: luhongjian@ncst.edu.cn(H.L.); Mouchao99@outlook.com(C.M.)

Abstract: The research on the excavation mechanical properties of underpass tunnels has already had certain results, but fewer of them consider the effects of dynamic and static loads on the excavation mechanical properties of underground tunnels at the same time, especially the lack of research cases of double-line highway tunnels with angled underpasses of existing railway tunnels. In this paper, based on the tunnel project of the new double-line Shiqian Highway Tunnel passing under the Hurong Railway at an oblique angle, the mechanical parameters of the rock body in the cross-tunneling area under the influence of static and dynamic load coupling are obtained by using the disturbance quantification coefficients and the Hoek-Brown criterion based on the method of over-advanced geological prediction and the investigation of the surrounding rock on the palisade face, and the engineering-scale finite element model is constructed and the mechanical characteristics of the excavation in the tunnel of the double-lane highway tunnel passing under the existing railroad under the influence of the static and dynamic loads are analyzed. The results show that: the new tunnel rock movement law for the top of the arch sinking, bottom plate bulging, side wall to move outward, the height and width of the arch and bottom plate arch with the tunnel excavation and increase, the side wall rock displacement effect is smaller; left and right lines of the tunnel disturbed area of the rule of change is similar; the existing tunnel bottom plate displacement is more than the top plate and the left and right side walls by the excavation of the time step influence is larger. Typical profile displacement is mainly determined by the distance from the excavation surface; the new tunnel in the four types of calculation conditions of the rock disturbance angle is the same; the existing tunnel roof and side wall Von Mises stress extreme occurs in the tunnel structure, the bottom plate there are pressure relief and pressure-bearing areas; based on the displacement control criteria, the recommended upper and lower step blasting method.

Keywords: tunnel underpass; effects of static and dynamic load coupling; numerical simulation; Hoek-Brown guidelines

1. Introduction

Underground highway and railway tunnels, as part of underground space development, are an important means of alleviating traffic congestion in China[1,2].With the gradual reduction of underground transportation space, new tunnels are often developed by going under existing tunnels[3,4].However, the excavation of new tunnels not only redistributes the stresses in the surrounding rock, but also increases the stresses and deformations in the existing tunnels due to secondary disturbances. Especially under the influence of dynamic loads of trains in the existing tunnel and dynamic and static loads of the excavated new tunnel, the tunnel structure will be further

　　doi:10.20944/preprints202403.1302.v1

2

deteriorated. The mechanical properties of the tunnel structure will be further deteriorated[5–8].Therefore, it is of great significance to study the mechanical characteristics of double-line new highway tunnels underneath the existing railway tunnels.

For the effect of excavating a new tunnel underpass on the mechanical properties of an existing tunnel, researchers often study it through theoretical derivation [9–11], model testing [12–14] and numerical simulation [15–19].

In terms of the static load effects of excavation,Chen et al. [15] investigated the effects of rock mass, radii of new and existing tunnels, burial depth of existing tunnels, and gaps between the traversing tunnels on the stability of existing tunnels by using the numerical simulation software FLAC3D (Itasca, 2017).In terms of oblique angle, Lin et al. [16] investigated the mechanical response of a new double-line tunnel passing under an existing tunnel at an oblique angle based on numerical simulation and verified it by on-site measurements. The results show that the diagonal angle undercutting will cause the lateral deformation and internal force of the existing tunnel to exhibit obvious asymmetric characteristics.Zhou et al. [20]investigated the effects of the shape of the tunnel, soil parameters and construction parameters on the ground settlement above the tunnel through numerical simulation. Chen et al. [21] systematically monitored the deformation and stress of the existing tunnel based on the case of a proximity earth pressure balance shield (EPBS) going down the existing tunnel. The results showed that the settlement development of the existing tunnels experienced four states: subsidence, bulge, secondary subsidence and stability, and the location of the maximum settlement point of the existing tunnels caused by the second tunnel underpass was biased towards the center of the twin tunnels.Lai et al. [22] used the finite difference method (FDM) to establish a model to study the settlement characteristics of the new tunnel with a small intersection angle close to the existing tunnel. The results show that the deformation of the existing tunnel caused by the excavation of the new tunnel is dominated by vertical settlement, accompanied by torsional deformation, and both deformations are the largest in the crossing area. The simulation results are consistent with the field monitoring data.Lei et al. [23] conducted a series of transparent clay modeling tests to study the effect of shield tunnel face excavation on the stability of existing tunnels. The results show that the damage mode of the shield tunnel face is an overall damage mode, and the relative vertical and horizontal distances play a dominant role in the damage mode.

In terms of the dynamic load impact of blasting and excavation of new tunnels, Cheng et al. [24] summarized the current research status of dynamic response, damage assessment and damage mitigation of highway tunnels under blast loads, and then discussed the effects of response analysis methods and response types on the dynamic response and damage characteristics of tunnel structures.Tian et al. [25] carried out a series of blasting vibration tests, and based on the actual engineering monitoring data, the tunnel blasting impact area was divided into four zones, which were the danger zone, warning zone, blasting control zone and safety zone. Then signal processing was carried out with the help of matlab programming, and the results showed that the maximum mass vibration velocity of the surface decreased with the increase of the distance, and the mass vibration velocity in the z-direction was greater than the mass vibration velocity in the horizontal direction.Duan et al. [26] analyzed the peak velocity change of particles, stress and settlement characteristics during the excavation of the cross-section of Gaojiu Road Ⅰ tunnel on the left line of Jiahua Tunnel based on field monitoring and numerical simulation. The results show that in the cross-section, the new tunnel blasting vibration has the greatest influence on the peak particle velocity at the roof of the existing tunnel below. The maximum tensile stresses in the existing tunnel below are mainly concentrated in the top region and the maximum compressive stresses are concentrated in the crown footing. The maximum cumulative settlement value is found at the cross-section of the two tunnels.Wu et al. [27] used ABAQUS simulation software to establish a tunnel blasting finite element model to study the vibration and stress response of the tunnel lining. The results show that in the same tunnel section, the vibration velocity response in the Y-direction is the largest and the vibration velocity response in the Z-direction is the smallest. The MISES stresses of the tunnel lining were distributed regionally.Ruan et al. [28] established a blasting vibration velocity model for deep rock mass and investigated the effect of overlying soil layer on blasting vibration. The results show that

the blasting vibration velocity gradually decreases with the increase of the thickness of the overburden layer.

Regarding the mechanical parameters of the rock mass in the influence area of the cross-tunneling project, some scholars have determined the rock mass reduction parameters based on the photo images and the information of the over-advanced geological prediction by using the Hoek-Brown criterion.Li et al. [29] established a more complete system of comprehensive tunnel overrun geological forecasting method, and established a comprehensive grading evaluation system for adverse geological conditions in tunnels.Zhou et al. [30] used the method of combining overpass geological prediction and palm face surrounding rock investigation to obtain the Hoek-Brown parameters of the tunnel surrounding rock, and then analyzed the stability of the surrounding rock in the fracture zone through FLAC~(3D) numerical simulation.Geng et al. [31]firstly determined the Hoek-Brown strength parameters by on-site investigation and empirical checklist method, and then simulated the excavation process of three-step method and double sidewall guideway method by combining FLAC3D. The results show that the double sidewall guideway method can better control the surrounding rock deformation and is suitable for tunnel sections with more broken surrounding rock.Hu et al. [32] corrected the parameters mb, s based on the Hoek-Brown strength criterion, from which the equivalent M-C strength parameters of anisotropic side-slope rock mass were further calculated, and the reasonableness of the parameters was tested by engineering examples.Li et al. [33] summarized the current research status of tunnel overtopping prediction technology by drill-and-blast method, and proposed a four-stage all-process integrated overtopping geological prediction system for tunnels.

To summarize, there are some results on the mechanical response characteristics of new tunnels with static excavation and blasting excavation, but usually the static and dynamic loads are only considered individually, and there are fewer cases that consider both at the same time, especially there is a lack of research cases on the tunneling of double-line highway tunnels diagonally passing through the existing railways. Therefore, this paper relies on the tunnel project of the new double-line Shiqian Highway Tunnel passing under the Hurong Railway at an oblique angle, adopts the method of over-advance geological prediction and palm face surrounding rock investigation, determines the rock mechanical parameters of the cross-tunneling project influence area considering the coupling effect of dynamic and static loads through the quantization of disturbance system and Hoek-Brown criterion, establishes the engineering-scale finite element numerical model, and reveals the mechanical parameters of the double-line highway tunnel passing through the existing railway tunnel under the influence of dynamic and static loads.

2. Project Background and Calculation Method

2.1. Project Background

This study relies on the cross-tunneling project of the double-line Shiqian Highway Tunnel with oblique angle under the Hurong Railway in the section of Wanshoushan.

Shiqian Highway Tunnel is a two-way four-lane tunnel with a total length of more than 90 kilometers, with a clear section width of 10.66m, a height of 8.60m, and a clear area of 76.85m². Hurong Wanshoushan Railway is a double-line tunnel with a total length of 264.4 kilometers, a one-sided gradient of 15.5%, a net section width of 12.26m, a height of 10.03m and a headroom area of 99.49m².

As shown in Figure 1, the road tunnel goes under the railway tunnel at an oblique angle of 61°, and the design line static spacing of the road tunnel at the underpass railway is 25m.
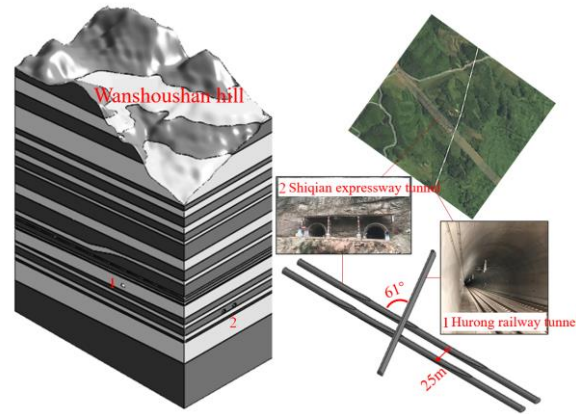
Figure 1. Spatial location map of the underpass tunnel project.

2.2. Calculation Method

In this paper, based on the results of the impact area of Wanshoushan double-line cross-tunnel project studied in the literature [34], the rock body in the impact area was optimized by adopting the method of optimizing the surrounding rock grading by using photo images and the information of the over-advanced geological prediction, using the disturbance coefficients to quantify the deterioration of the rock properties caused by the static and dynamic load, and determining the mechanical parameters of the rock body in the impact area of the cross-tunnel project by taking into consideration of the influence of the dynamic and static load coupling with the application of Hoek-Brown criterion, which in turn revealed the mechanical characteristics of the excavation for the tunnel of the double-line highway tunnel under the influence of the dynamic and static load under the influence of the tunnel crossing the existing railway.

2.2.1. Hoek-Brown Guidelines

The Hoek-Brown criterion is an empirical guideline for determining the mechanical parameters of a rock mass and includes the GSI geostrength index and the rock disturbance coefficient D.

The expression for the Hoek-Brown empirical criterion [35] is:

$$\sigma_1 = \sigma_3 + \sigma_{ci}[m_b(\sigma_3/\sigma_{ci}) + s]^a \tag{1}$$

where σ_1 and σ_3 are the maximum and minimum principal stresses, σ_{ci} is the uniaxial compressive strength of the rock mass, and m_b, s, and a are the semi-empirical parameters of rock properties as a function of the Geological Strength Index GSI [36]:

$$m_b = m_i e^{[(GSI-100)/(28-14D)]} \tag{2}$$

$$s = e^{[(GSI-100)/(9-3D)]} \tag{3}$$

$$a = 1/2 + (e^{-GSI/15} - e^{-20/3})/6 \tag{4}$$

$$GSI = 1.5 Jcond_{89} + RQD/2 \tag{5}$$

In the formula, $Jcond_{89}$ is the state of joints, RQD is the quality of rock, GSI is the geological strength index, the three take values in the range of 5~100; m_i is the rock material constant, obtained from the triaxial compression test of intact rock, can also be determined according to the type of rock, the structure, take the value of the range of 5~40; D is the weakening factor for the consideration of the rock body by anthropogenic or natural factors of perturbation, take the value of the range of 0~1.

1) Determination of modulus of elasticity

The modulus of elasticity is an important parameter describing the strength of a material, and the modulus of elasticity E_m (GPa) of a rock is calculated as:

$$E_m = (1-0.5D) \cdot (\sigma_{ci}/100)^{0.5} \cdot 10^{[(GSI-10)/40]}, \quad \sigma_{ci} \leq 100MPa \tag{6}$$

$$E_m = (1-0.5D) \cdot 10^{[(GSI-10)/40]}, \quad \sigma_{ci} > 100MPa \tag{7}$$

2) Determination of shear strength parameters

The shear strength parameters are cohesion c and friction angle φ. The expressions for the equivalent cohesion c' and equivalent friction angle φ' of the rock adopted by the Hoek-Brown criterion are, respectively:

$$c' = \frac{\sigma_{ci}[(1+2a)s+(1-a)m_b\sigma'_{3n}](s+m_b\sigma'_{3n})^{a-1}}{(1+a)(2+a)\sqrt{1+[6am_b(s+m_b\sigma'_{3n})^{a-1}]/[(1+a)(2+a)]}} \tag{8}$$

$$\varphi' = \arcsin[\frac{6am_b(s+m_b\sigma'_{3n})^{a-1}}{2(1+a)(2+a)+6am_b(s+m_b\sigma'_{3n})^{a-1}}] \tag{9}$$

where $\sigma'_{3n}=\sigma'_{3\max}/\sigma_{ci}$, and for deep tunnels $\sigma'_{3\max}$ can be determined by the following equation:

$$\sigma'_{3\max}/\sigma'_{cm} = 0.47(\sigma'_{cm}/\gamma H)^{-0.94} \tag{10}$$

where γ is the bulk weight of the rock mass; H is the burial depth of the tunnel, and when the horizontal stress is higher than the vertical stress, γH in Eq. (10) is replaced by the value of the horizontal stress; σ'_{cm} is the strength of the rock mass, which is calculated by the formula:

$$\sigma'_{cm} = \sigma_{ci}\frac{[m_b+4s-a(m_b-8s)](0.25m_b+s)^{a-1}}{2(1+a)(2+a)} \tag{11}$$

(3) Disturbance factor of rock mass for tunneling D

The disturbance factor for the rock mass is usually taken empirically, as shown in Table 1.

Table 1. Table of rock disturbance coefficients in tunneling.

| Description of rock excavation methods and effects	D value
Very little disturbance, good blasting or tunnel boring machine excavation	0
Small disturbances, poor rock mass with mechanical or manual excavation	0
Large disturbances, stress concentrations causing the tunnel bottom to bulge	0.5
High disturbance, poor blasting results	0.8

2.2.2. Determination of Rock Reduction Parameters

1)Hoek-Brown criterion parameterization

(1)GSI value determination

The Hoek-Brown criterion parameters were determined on the basis of the distribution profiles of rock layers and surrounding rock grades in the new tunnels, the overtopping geological forecast, and the observation information of the palm face, combined with the GSI index map proposed by Hoke et al [36].

a.Rock layer and surrounding rock grading section

The new Wanshoushan Tunnel is a double-line highway tunnel, the left line intersects with Hurong Railway Tunnel at K3+674.943 (Figure 2 L₀), and the right line intersects with Hurong Railway Tunnel at YK3+694.291 (Figure 3 R₀). The 60m before and after the intersection point of the new highway tunnel is the excavation sensitive area [34], as shown in Figure 2-2. Preliminarily, the excavation sensitive area is determined as Class IV surrounding rock. Typical cross-sections of 60m and 85m before and after the tunnel intersection are extracted for analysis, the left line: L1 section K3+590, L2 section K3+615, L3 section K3+735, L4 section K3+760, and the right line: R1 section YK3+609, R2 section YK3+634, R3 section YK3+754, R4 section YK3+779.
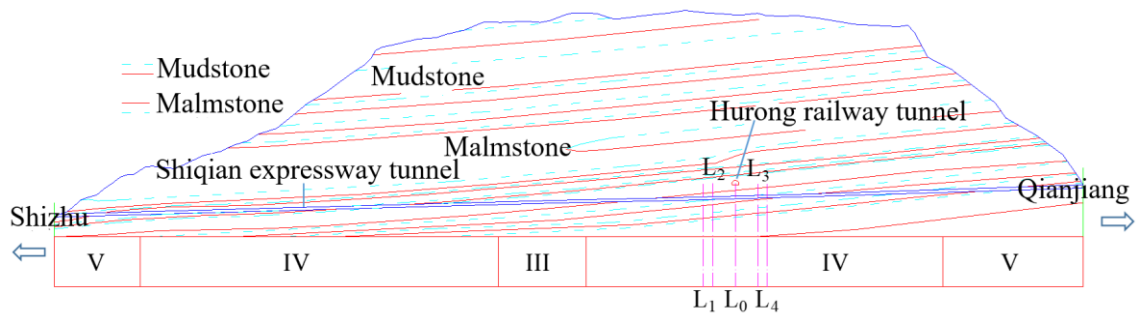
Figure 2. Grading section of rock strata and surrounding rocks in the left lane of the new tunnel.
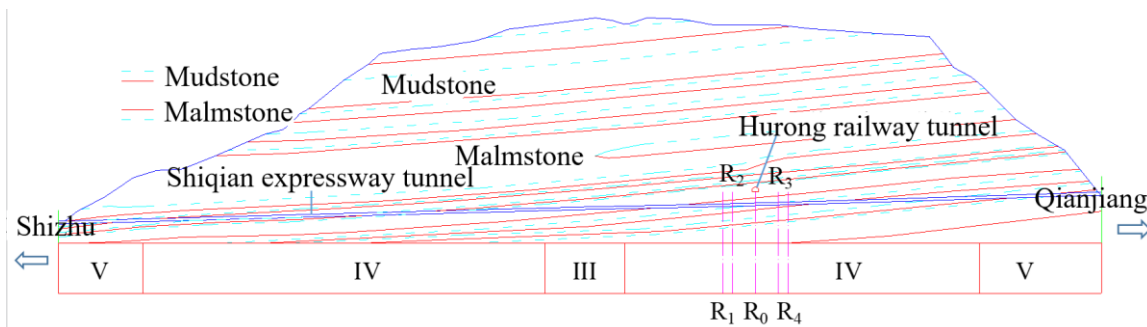

Figure 3. Grading section of rock layers and surrounding rocks in the right lane of the new tunnel.

b. Over-advanced geological forecast

The equipment used for advanced geological forecasting is SRI-20 geological radar combined with 100MHz antenna, as shown in Figure 4. The geological forecast line is 12m long and distributed in the shape of a zigzag at the bottom of the upper step of the palm face, 1.2m away from the height of the lower step (Figure 5).

Figure 4. Over-the-top geological forecasting SIR-20 geological radar with 100 MHz antenna.
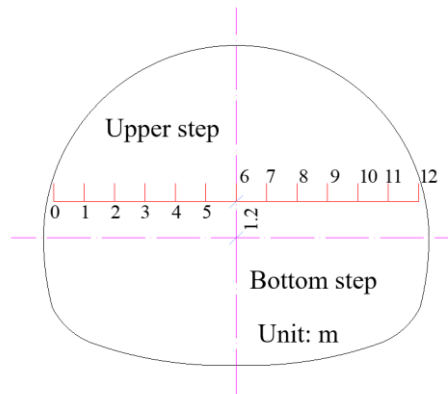
Figure 5. Layout of the over-advanced geological forecast line.

c. Left line palm surface observation and radar data analysis

Photographs of the palm faces of the four sections of the left line are shown in Figures 6–9.

Figure 6. L_1 Photographs of sectioned palm faces.

Figure 7. L_2 Photographs of sectioned palm faces.

The surrounding rocks of L1 and L2 sections are mainly medium-weathered grayish-white malmstone, with good integrity and interlayer combination, undeveloped joints and fissures, and a dry palm surface. a small amount of mudstone locally exists in L1, with medium-thickness bedding, and thick bedding is dominant in L2.

Figure 8. L3 Photographs of sectioned palm faces.

**Figure 9.** L4 Photographs of sectioned palm faces.

The surrounding rock of L3 section is mainly mudstone, which is soft rock. The rock body is relatively broken, mainly in thin layers, the combination between rock layers is general, joints and fissures are developed, strong weathering is dominant, and the palm surface is dry.

The surrounding rocks in section L4 are mainly mudstone, and there are obvious malmstone and mudstone interlayers within 2m above the upper step, of which mudstone is soft rock and malmstone is hard rock. The rock body is more complete, the combination between the rock layers is general, the joints and fissures are developed, medium weathering is dominant, and the palm surface is drier.

The data analysis of the left line radar over-advanced geological forecast is shown in Figures 10–13.
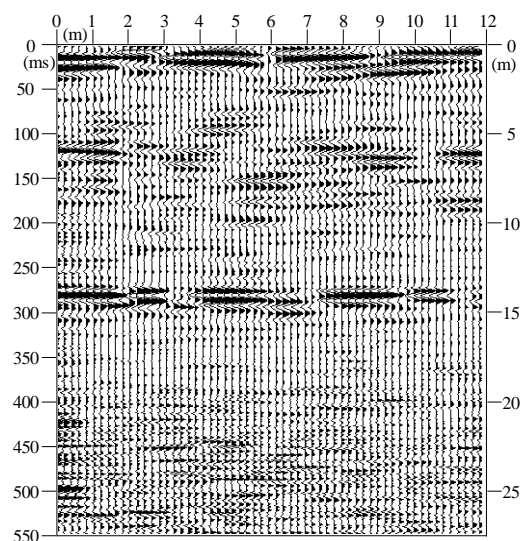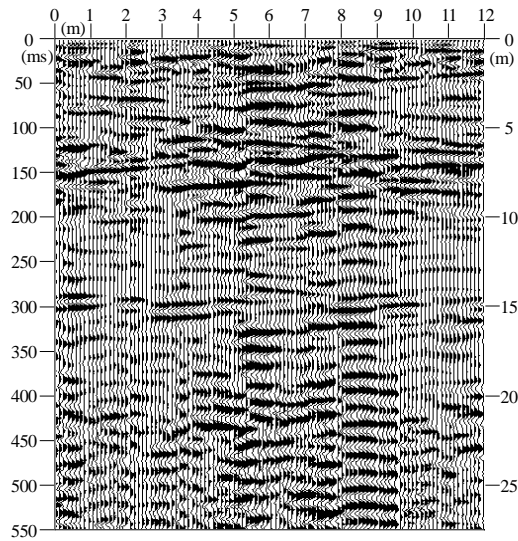

Figure 10. L1 Cross-section radar data analysis map.
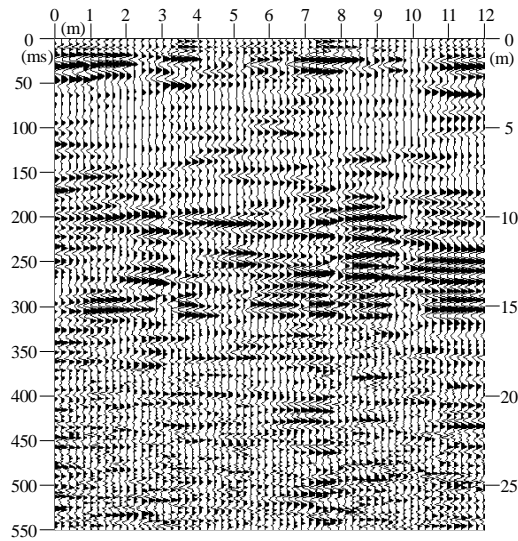
Figure 11. L2 Cross-section radar data analysis map.

The radar reflection signals of L1 and L2 sections are strong, and the frequency change of electromagnetic wave signals is general and continuous in the same direction, L1 is dominated by medium-low frequency signals, and L2 is dominated by medium-high frequency signals. Combined with the condition of the palm surface of the section, it is concluded that the 0~25m section in front of the L1 and L2 section is mainly malmstone, which belongs to the harder rock, the joints and fissures are not developed, and the integrity of the rock body is better, and it is the IV level of preferred surrounding rock.
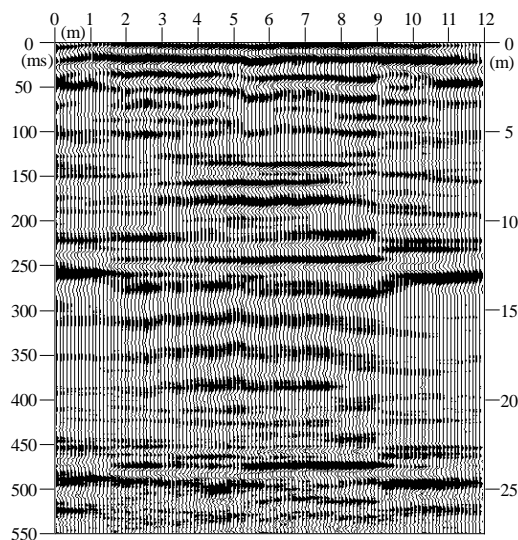

Figure 12. L3 Cross-section radar data analysis map.

Figure 13. L4 Cross-section radar data analysis map.

L3 section radar reflection signal is strong, electromagnetic wave signal frequency change is general, mainly in the middle and high frequency signal, isotropic axis intermittent, local continuous, no obvious shock wave signal. Combined with the situation of palm surface in L3 section, it is concluded that mudstone is dominated in the range of 0~25m in front of L3 section, which is soft rock, with joints and fissures developed, and the integrity of surrounding rock is general, and there are weak and soft surrounding rock segments in the local area, and it is a class IV deviation surrounding rock.

The radar reflection signal of L4 section is strong, and the frequency change of electromagnetic wave signal is general, dominated by homogeneous medium-low frequency signal, with continuous isotropic axis and no obvious shock wave signal. Combined with the situation of the palm face of L4 section, it is concluded that mudstone is dominant in the range of 0~25m in front of L4 section, and there may be malmstone and mudstone interbedding in the local area, of which mudstone is soft rock and malmstone is harder rock, with joints and fissures developed, and the integrity of surrounding rock is general, and it is class IV surrounding rock.

d.Observation and radar data analysis of the right line palm surface

Photographs of the palm faces of the four sections of the right line are shown in Figures 14–17.
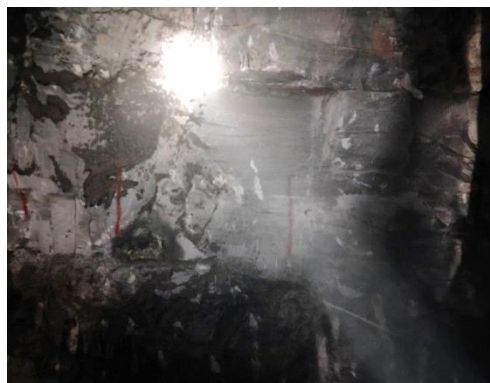
Figure 14. R1 Photographs of sectioned palm faces.

Figure 15. R_2 Photographs of sectioned palm faces.

Figure 16. R_3 Photographs of sectioned palm faces.

Figure 17. R_4 Photographs of sectioned palm faces.

The surrounding rocks in section R1 are mainly gray-white malmstone, the rock body is complete, mainly medium-thick laminated, the combination between the rock layers is good, the joints and fissures are not developed, mainly medium weathering, and the palm face is dry.

The surrounding rocks in section R2 are mainly malmstone, mixed with mudstone, malmstone is soft rock, mudstone is soft rock, and there is obvious interlayer in the middle of the palm face. The surrounding rocks are mainly medium-thick bedded, the integrity of the rock body is general, the combination between the rock layers is general, the joints and fissures are developed, strong weathering is dominant, and the palm surface is dry.

The surrounding rocks in section R3 are mainly mudstone and malmstone, mudstone is soft rock and malmstone is hard rock. The rock body is more broken, mainly in thin layers, and the combination between the rock layers is poor.

R4 section is mainly surrounded by mudstone, which is soft rock, surrounded by thin layer, the integrity of rock body is general, and the combination between rock layers is general~better.R3 and

R4 sections have developed joints and fissures, which are mainly strongly weathered, and the palm surface is dry.
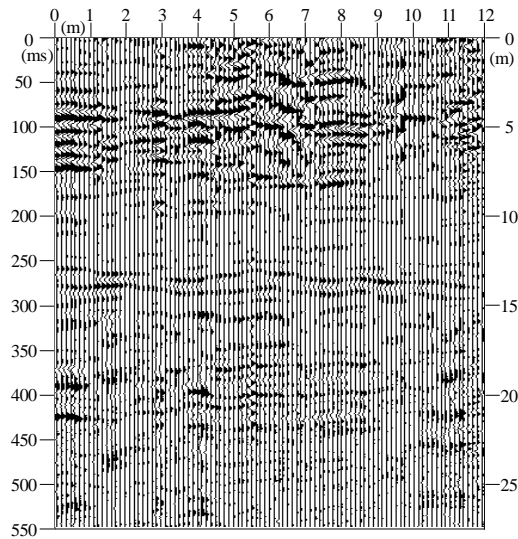
The right line radar overpass geological forecast data analysis, as shown in Figures 18–21.
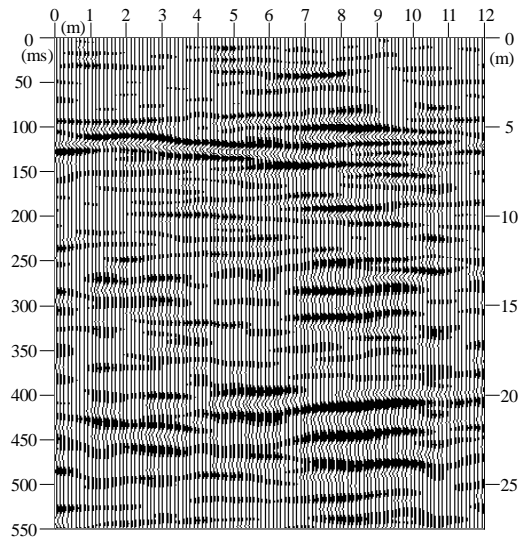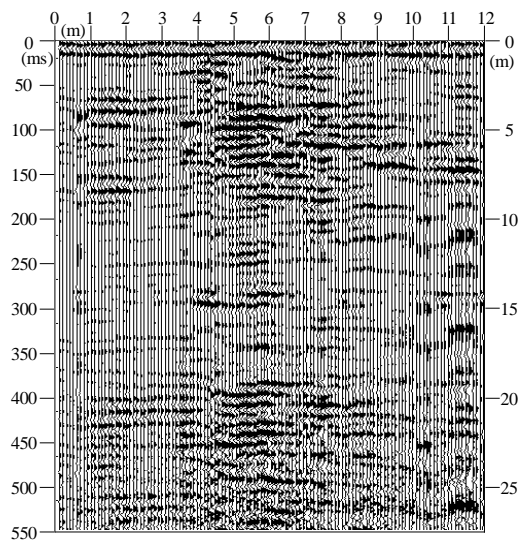

Figure 18. R_1 Cross-section radar data analysis map.
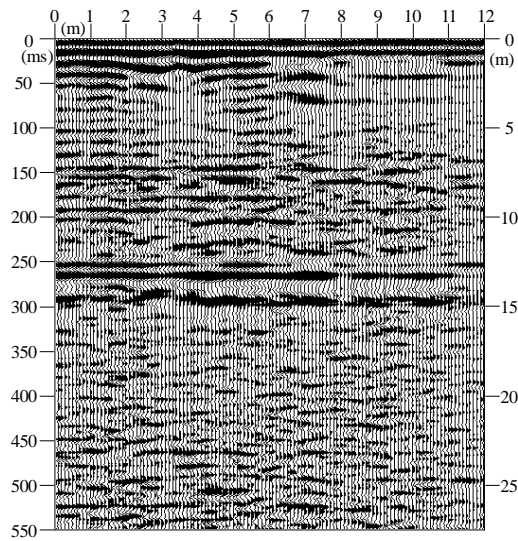
Figure 19. R_2 Cross-section radar data analysis map.

Figure 20. R3 Cross-section radar data analysis map.

Figure 21. R4 Cross-section radar data analysis map.

The radar reflection signal is stronger in section R1 and weaker in section R2.R1 and R2 electromagnetic wave signal frequency change is general, mainly in low frequency signal, isotropic axis intermittent, combined with the section palm surface of the situation of R1 and R2 section in front of the 0~25m section to malmstone is dominated by the malmstone, mixed with mudstone, malmstone belongs to the softer rock, mudstone belongs to the soft rock. The joints and fissures are developed, and the rock body integrity is general, which is class IV surrounding rock.

R3 section radar reflection signal is strong, the electromagnetic wave signal frequency change is general, mainly in the middle and high frequency signal, the same direction axis is locally continuous, locally intermittent, the amplitude is general. Combined with the situation of R3 section palm face, it is concluded that 0~25m range in front of R3 section is dominated by mudstone and malmstone, mudstone belongs to soft rock, malmstone belongs to hard rock, joints and fissures are developed in the range of 0~10m in front of palm face, and the integrity of peripheral rock is general, and it is the peripheral rock of IV level deviation.

The radar reflection signal of R4 section is strong, and the frequency change of electromagnetic wave signal is general, dominated by medium and high frequency signal, with the same direction axis continuous, without obvious shock wave signal. Combined with the situation of R4 section palm

face, it is concluded that the range of 0~25m in front of R4 section is dominated by mudstone, which is soft rock, with undeveloped joints and fissures, and the integrity of surrounding rock is general, and it is a class IV deviation surrounding rock.

The photo of the new tunnel palm face and the result of the analysis of the overtopping geological prediction radar data are in good agreement with the grading profile of the rock layers and the surrounding rocks. Therefore, it is finally determined that the malmstone layer of the cross-tunnel project (assuming that the grading of the surrounding rocks of the existing tunnels is the same as that of the new tunnels) is a Class IV preferred surrounding rock and the mudstone layer is a Class IV deviated surrounding rock, and at the same time, with reference to the GSI index diagram (Figure 22), it is determined that the malmstone and mudstone layers have a GSI value of 55 and 45.
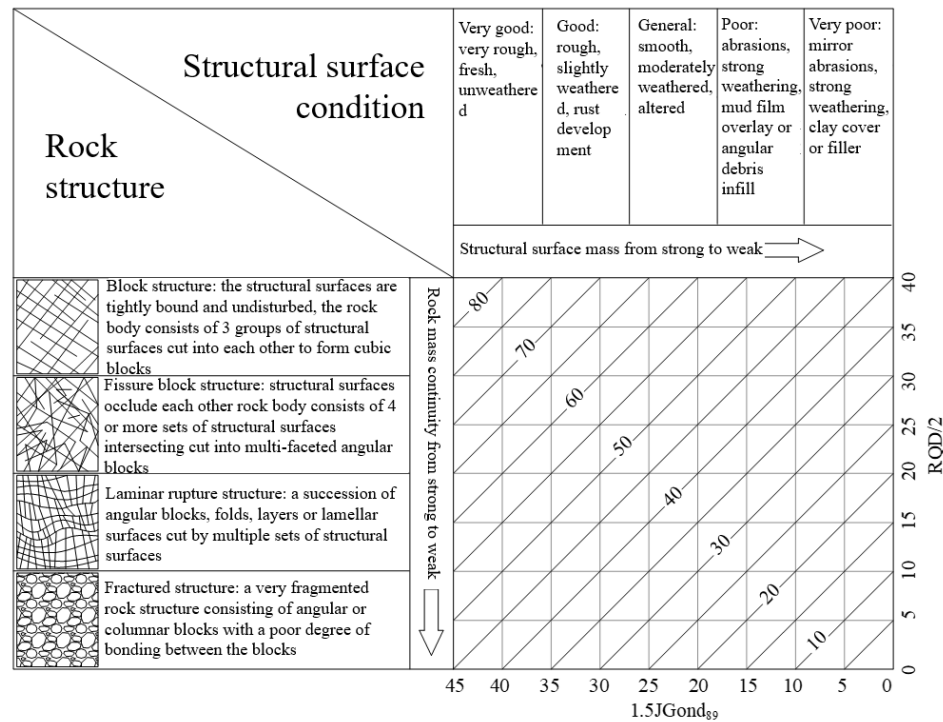

Figure 22. GSI indicator identification chart.

(2)Determination of rock integrity coefficient m_i

Based on the palm face observation and overtopping geological forecast information, the integrity coefficient of rock m_i was determined by rock type and structure[36] (Table 2), and the integrity coefficients of malmstone and mudstone formations of the cross-tunneling project were determined to be 21 and 9.

Table 2. Classification table of rock integrity coefficients m_i.

Rock Type	Rock group	Rock structure			
		Coarse	Medium grain	Grain	Very fine grain
Sedimentary rock	Clastic rock	Conglomerate (geology)	Malmstone	Conglomerate (geology)	Malmstone
		17±4 siltstone		17±4 siltstone	
	Non-clastic rocks	7±2Claystone		7±2Claystone	
	Carbonate rock	4±2		4±2	
	Non-clastic rocks	Conglomerate		Conglomerate	
Metamorphic	EvaporitesNon-clastic rocks		- miscellaneous malmstones		- miscellaneous malmstones
		(18±3) Shale		(18±3) Shale	

	Organic Rocks	6±2	6±2	
	Non-fragmentary	Marl (7±2)	Marl (7±2)	
	Microfacies	Coarse crystalline limestone		Coarse crystalline limestone
Volcanic rock	Lamellar Light-colored,dark-octidolite	(12±3) Brilliant limestone (10±2) Microcrystalline limestone	(12±3) Brilliant limestone	(10±2) Microcrystalline limestone
	Dark colored plutonic rocks	(9±2) Dolomite (9±2) Dolomite Gypsum rock	(9±2) Dolomite (9±2) Dolomite Gypsum rock	
	Light-colored, dark-colored mafic rocks	8±2 Hard gypsum	8±2 Hard gypsum	

(3) Determination of uniaxial compressive strength σ_{ci} of rocks

Test uniaxial compression test is carried out to determine the uniaxial compressive strength of malmstone and mudstone of cross tunnel project as 8.9 MPa and 3.84 MPa respectively.

(4) Determination of disturbance coefficient D

Based on the disturbance situation of the field tunnel[34], referring to the rock disturbance coefficient value chart (Table 1), it is determined that the disturbance coefficient of the area affected by blasting and excavation of the cross-tunnel project is 0.5, that of the area affected by static excavation is 0, that of the area affected by the train dynamic load is 0.2, and that of the area overlapping the blasting load and the train dynamic load is 0.7.

(5) Determination of rock mass related parameters for cross-tunneling project

The average depth of the new tunnel is 460m, the average depth of the existing tunnel is 420m, the average depth of the overlapping area is 445m, and the average weight of the overlying rock layer takes the average value of the weight of malmstone and mudstone to be 23.51kN/m³. The values of GSI, m_i, σ_{ci}, D, γ, and H will be brought into the corresponding formulas, which will result in the values of the relevant parameters of the rock body in the area affected by the cross-tunneling project, and the details are shown in Table 3.

Table 3. Table of relevant parameters for each rock type in the area of influence.

Area of influence	Excavation method	Rock type	m_b	s	a	σ'_{cm}/MPa	σ'_{3n}/MPa
New tunnels	Blasting excavation	Malmstone	2.464	0.0025	0.504	1.86	0.514
		Mudstone	0.656	0.0007	0.508	0.40	1.087
	Static excavation	Malmstone	4.210	0.0067	0.504	2.46	0.523
		Mudstone	1.262	0.0022	0.508	0.57	1.109
Existing tunnels	— —	Malmstone	3.521	0.0047	0.504	2.24	0.477
		Mudstone	1.015	0.0014	0.508	0.51	1.011
Overlap zone	Blasting excavation	Malmstone	1.772	0.0015	0.504	1.57	0.493
		Mudstone	0.438	0.0003	0.508	0.33	1.040
	Static excavation	Malmstone	3.521	0.0047	0.504	2.24	0.504
		Mudstone	1.015	0.0014	0.508	0.51	1.068

2) Determination of mechanical parameters of rock body

The values of the relevant parameters in Table 3 of the rock mass and literature [34] were brought into the previous equations to derive the parameters of elastic modulus, equivalent cohesion,

equivalent internal friction angle and Poisson's ratio for different influence regions [37], which are detailed in Table 4.

Table 4. able of mechanical parameters for rock modeling in different regions of influence.

Area of influence	Excavation method	Rock type	γ	E/GPa	c'/MPa	φ'/°	v
New tunnels	Blasting excavation	Malmstone	23.13	2.98	0.80	27.90	0.27
		Mudstone	23.89	1.10	0.33	13.77	0.38
	Static excavation	Malmstone	23.13	3.98	0.97	32.23	0.23
		Mudstone	23.89	1.47	0.44	17.53	0.35
Existing tunnels	— —	Malmstone	23.13	3.58	0.86	31.48	0.24
		Mudstone	23.89	1.32	0.38	16.72	0.36
Overlap zone	Blasting excavation	Malmstone	23.13	2.59	0.69	25.60	0.28
		Mudstone	23.89	0.96	0.27	11.91	0.40
	Static excavation	Malmstone	23.13	3.58	0.89	31.03	0.24
		Mudstone	23.89	1.32	0.39	16.39	0.36

## 3. Three-Dimensional Numerical Model

3.1. Model Building

The mechanical parameters of the rock body in different influence areas are brought into the Wanshoushan double-line cross tunnel engineering model to get the mechanical characteristics analysis grid model of the tunnel excavation under the existing railway, as shown in Figure 23.
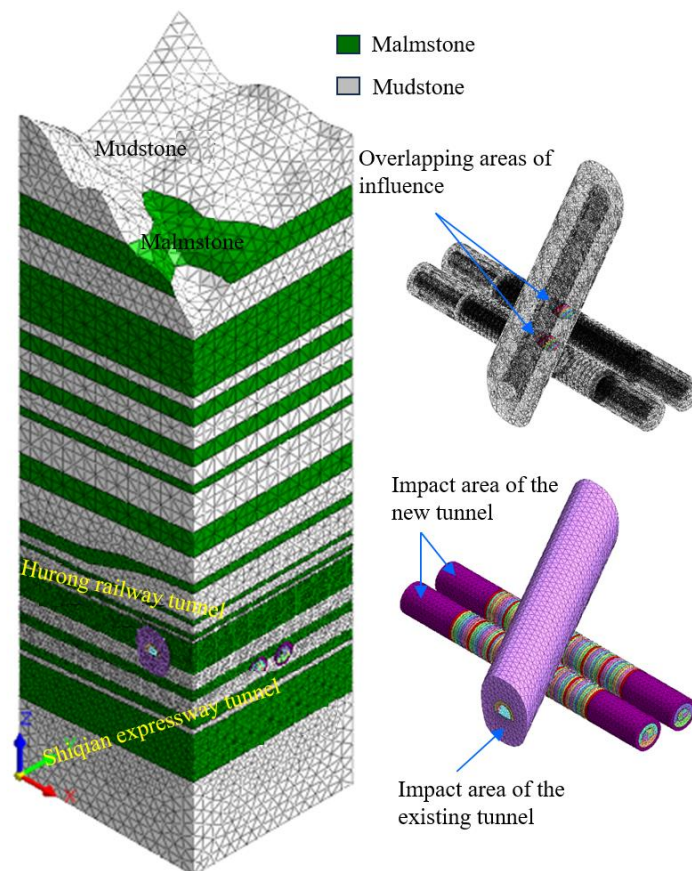

Figure 23. Grid model for mechanical characterization of tunnel excavation under double-line highway tunnel passing through existing railway.

3.2. Calculation of Working Conditions

Combined with the design of the tunnel excavation in the cross section, four working conditions are selected for the mechanical characterization of the excavation methods in the influence area, and the numerical calculation conditions are: upper and lower step blasting method excavation (UPBM), upper and lower step static method excavation (UPSM), CD blasting method excavation (CDBM), and CD static method excavation (CDSM) as shown in Figure 24 and Figure 25, and blasting and static method excavation is realized based on the mechanical parameters of the rock body computed by the different perturbation coefficients D in the Hoek-Brown criterion.
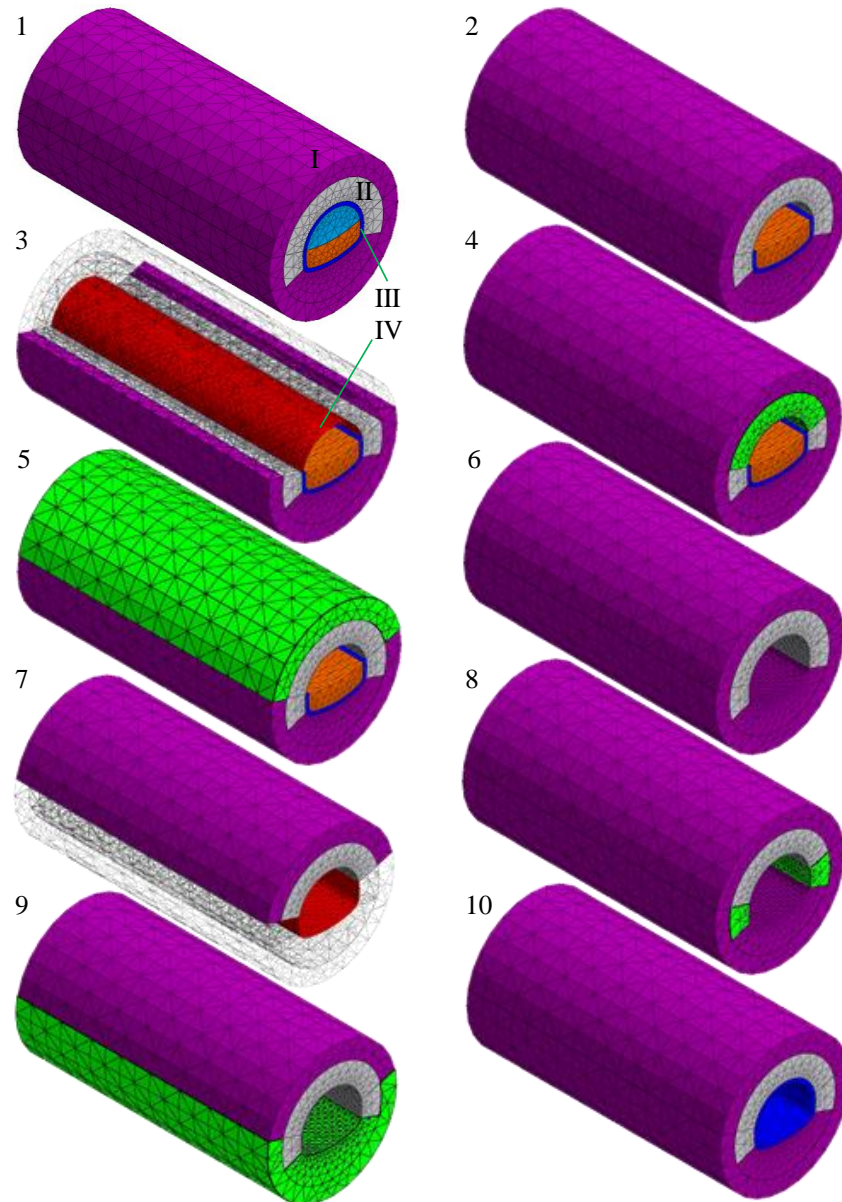
Figure 24. Upper and lower step method excavation process grid model diagrams: I - new tunnel blasting excavation influence area, II - anchor reinforcement area, III - secondary lining support, IV - initial support; 1 - pre-excavation cross-section, 2 - upper step excavation, 3 - upper step initial support, 4 - upper step anchor reinforcement area imposition, 5 - upper step peripheral rock influence area imposition, 6 - lower step excavation, 7 - lower step initial support, 8 - lower step anchor reinforcement area imposition, 9 - lower step peripheral rock influence area imposition, 10 - secondary lining support.

18
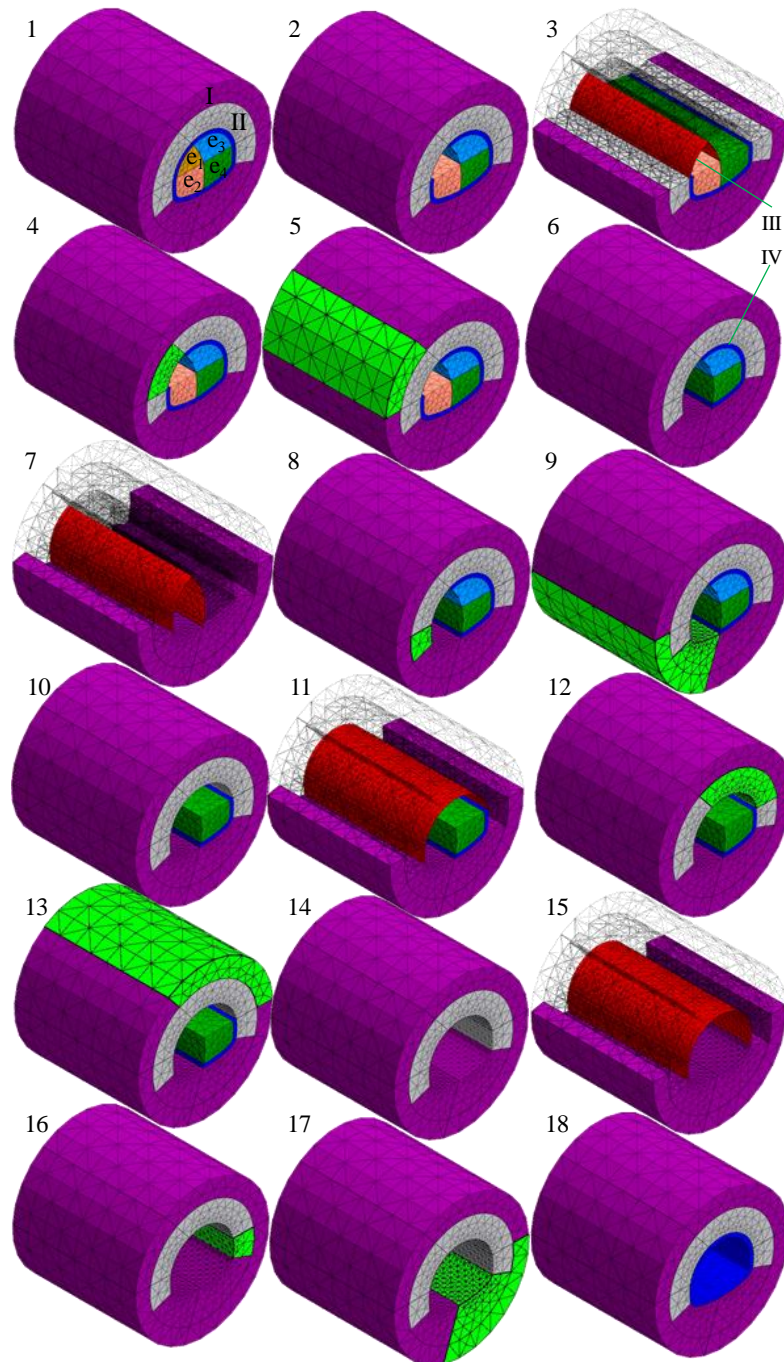
Figure 25. Grid model diagram of excavation process of CD method: I - blasting excavation influence area of new tunnel, II - anchor reinforcement area, III - secondary lining support, IV - initial support, e1 - left upper guide pit area, e2 - left lower guide pit area, e3 - right upper guide pit area, e4 - right lower guide pit area; 1 - pre-excavation cross-section view, 2 - left upper guide pit excavation, 3 - left upper guide pit initial support, 4- left upper guide pit anchor reinforcement zone applied, 5- left upper guide pit perimeter rock influence zone applied, 6- left lower guide pit excavation, 7- left lower guide pit initial support, 8- left lower guide pit anchor reinforcement zone applied, 9- left lower guide pit perimeter rock influence zone applied, 10- right upper guide pit excavation, 11- right upper guide pit initial support, 12- right upper guide pit anchor reinforcement zone imposed, 13- Right side upper guide pit perimeter rock influence zone imposed, 14- Right side lower guide pit excavation, 15- Right side lower guide pit initial support, 16- Right side lower guide pit anchor reinforcement zone imposed, 17- Right side lower guide pit perimeter rock influence zone imposed, and 18- Secondary lining support.

19

The left line tunnel is set as the first excavation tunnel, which is excavated from the inlet (left) to the outlet (right). In order to reduce the boundary effect, the excavation process of the new tunnel is carried out in 140m in the analyzed area, and the extracted time-steps Si are numbered as S1, S2, S3, ...S10, and the left and right line tunnels differ by 3 Si , and the length of Si is 20m, as shown in Figure 26.
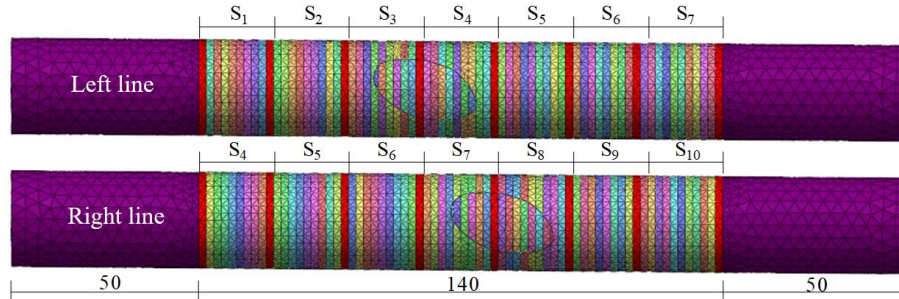

Figure 26. Tunnel excavation data extraction time step diagram.

4. Results

### 4.1. Analysis of Rock Formations in the Area of Influence

Tunnel excavation and support will change the displacement and stress of the initial stress field of the surrounding rock and form a new equilibrium stress field. In order to reveal the mechanical response mechanism of the underpass tunnel excavation project, the total displacement and Von Mises stress evolution characteristics of the cross-tunneling project are analyzed by extracting different time-step data as an example of the working condition of the upper and lower step blasting method.

4.1.1. Total Displacement Response

The total displacement response characteristics of the cross-tunneling project were analyzed based on the vector and total displacement cloud maps of the axial profile of the new left-lane tunnel and the axial profile of the existing tunnel, and the monitoring point data.

1)Vector versus total displacement cloud analysis

Figure 27 shows the axial profile vector and total displacement of the new left tunnel. After the excavation and support of the new tunnel, the upper rock layer moves downward and the bottom rock layer moves upward. The displacement affected area is divided into strong disturbance area I, medium disturbance area II, low disturbance area III and slight disturbance area IV, which are symmetrically distributed.
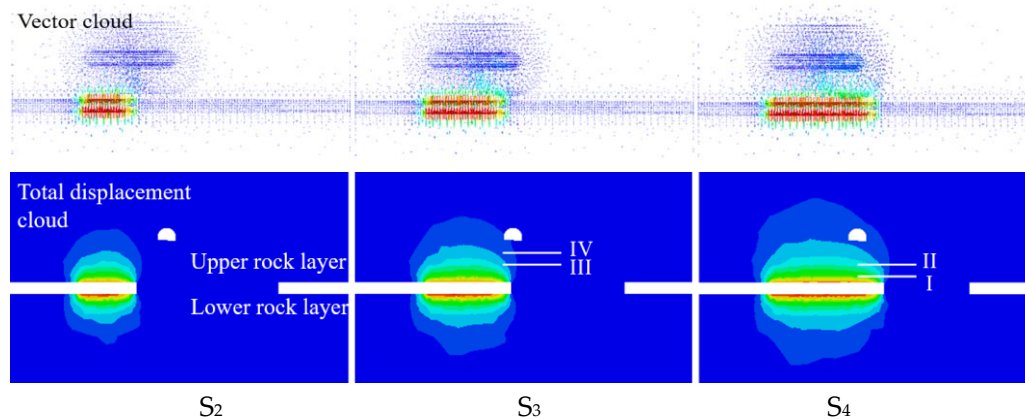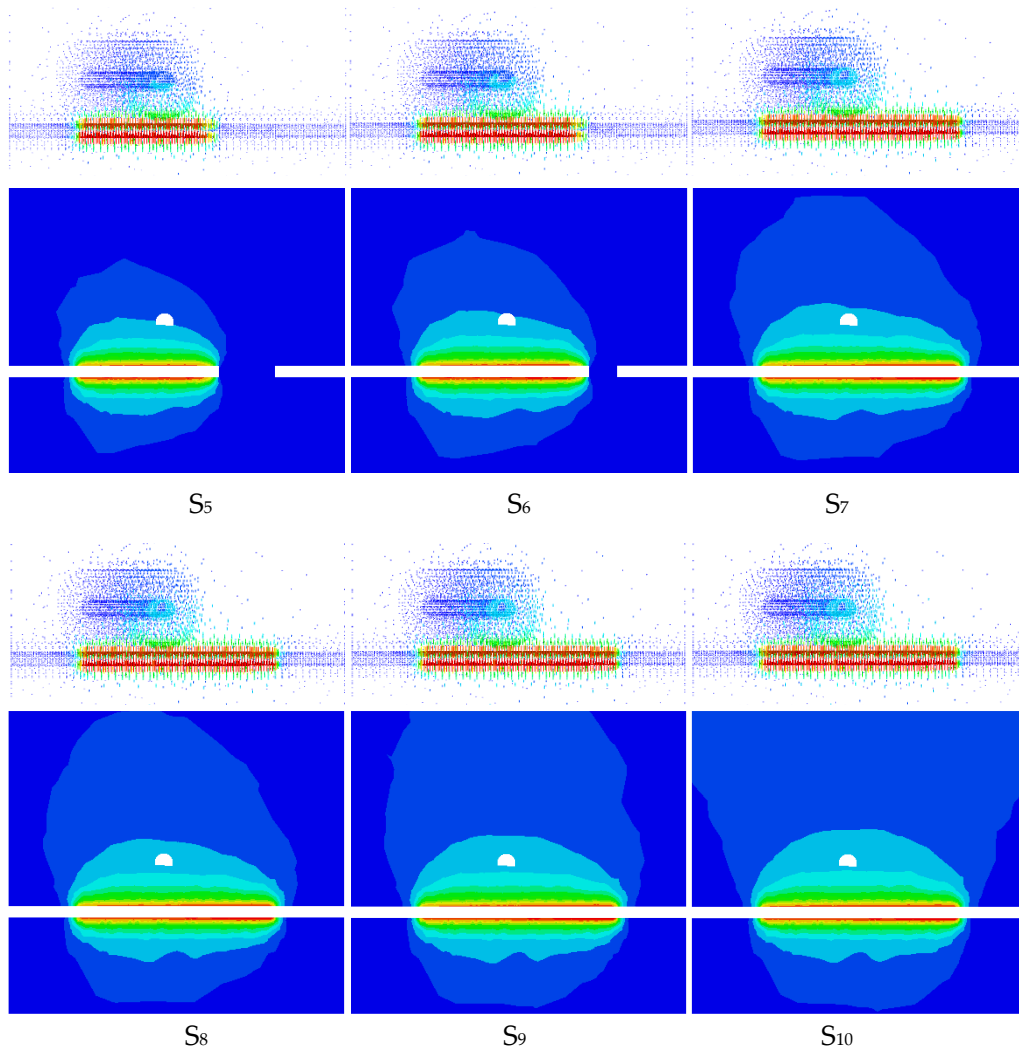
Figure 27. New axial profile vector and total displacement cloud map of left tunnel.

As the excavation progresses, the range of each influence area tends to increase. In the upper rock layer, the strong disturbance area ranges from 1 to 2 times the diameter of the hole, the medium disturbance area ranges from 0.5 to 1 times the diameter of the hole, the low disturbance area ranges from 0.8 to 3.5 times the diameter of the hole, and the micro-disturbance area has a large range. In the bottom rock layer, the strong disturbance region ranges from 1 to 1.5 times the hole diameter, the medium disturbance region ranges from 0.5 times the hole diameter, the low disturbance region ranges from 0.5 to 2 times the hole diameter, and the micro-disturbance region ranges from 2 to 4 times the hole diameter.

Figure 28 shows the axial profile vector and total displacement cloud diagram of the existing tunnel. After the excavation and support of the new tunnel, the tunnel vault sinks, the floor slab bulges, and the side walls move outward. The displacement areas of the upper and lower rock layers of the new tunnel include four areas: strong disturbance area I, medium disturbance area II, low disturbance area III, and micro-disturbance area IV, while the displacement areas of the rock layers of the sidewalls are mainly in the two areas of low-disturbance area III and micro-disturbance area IV.
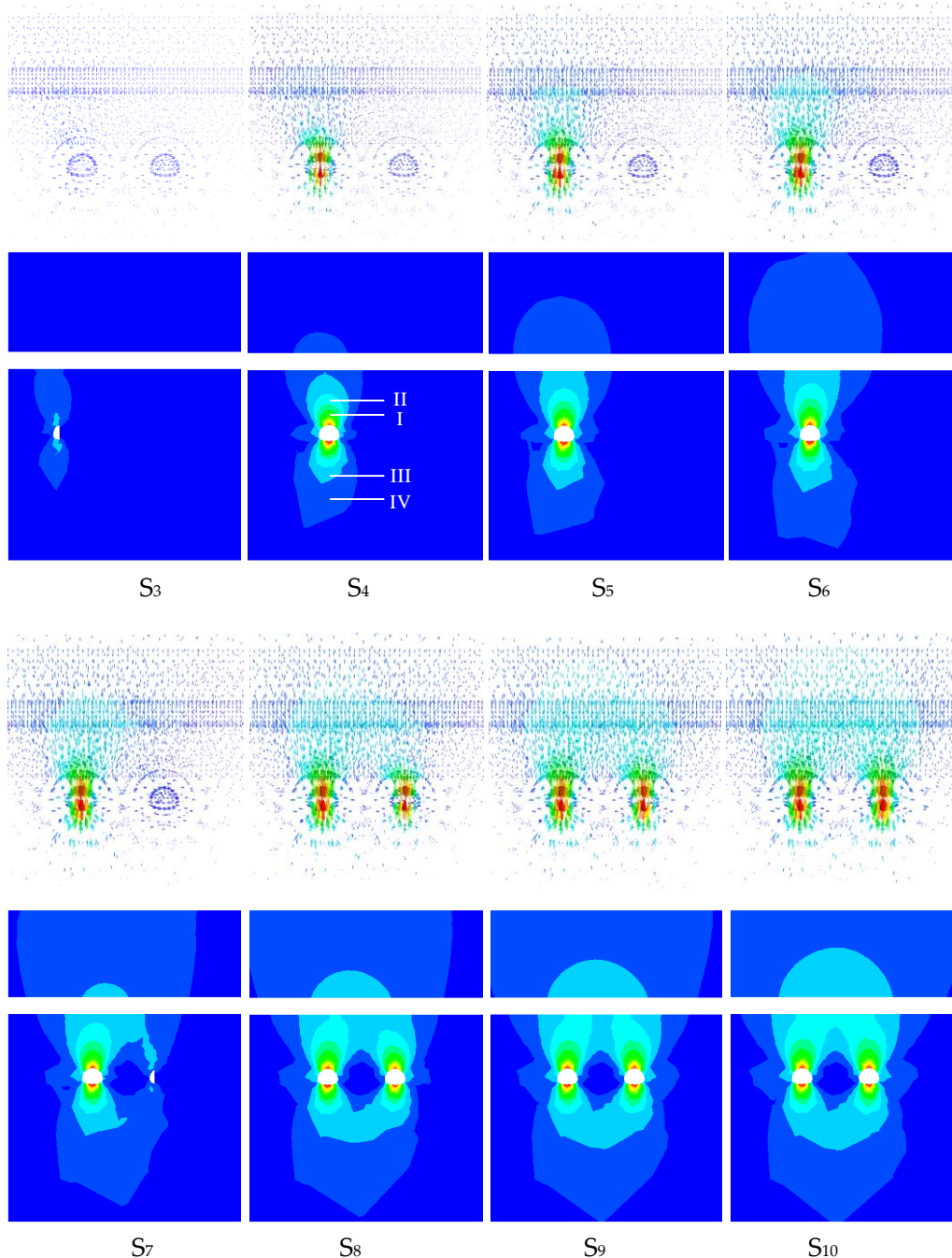
Figure 28. Vector and total displacement maps of the axial section of the existing tunnel.

As the tunnel excavation progresses, the height and width of the upper and lower arch influence zones of the tunnel increase, while the lateral direction does not change much. The left tunnel and right tunnel excavation and support process of strong disturbance area and medium disturbance area have similar change rules, and expand separately; low disturbance area and micro-disturbance area are based on the basis of the first excavation impact area to expand in concert; the middle area of the tunnel exists in the micro-disturbance and undisturbed area.

2) Analysis of monitoring point data

Five typical profiles are selected at an interval of 17.85m in the Y-axis direction of the cross-tunneling project, and four 24m-long survey lines are arranged in each profile, and five survey points at an interval of 6m are arranged on each survey line, as shown in Figure 29.
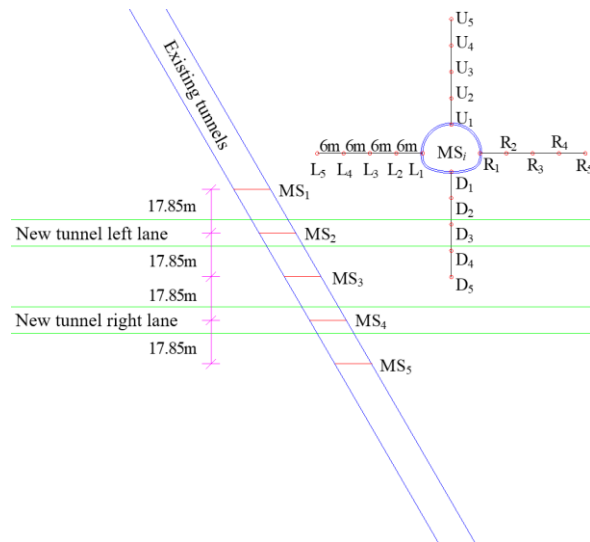
Figure 29. Typical Y-axis profile and survey point layout of cross-tunneling project.
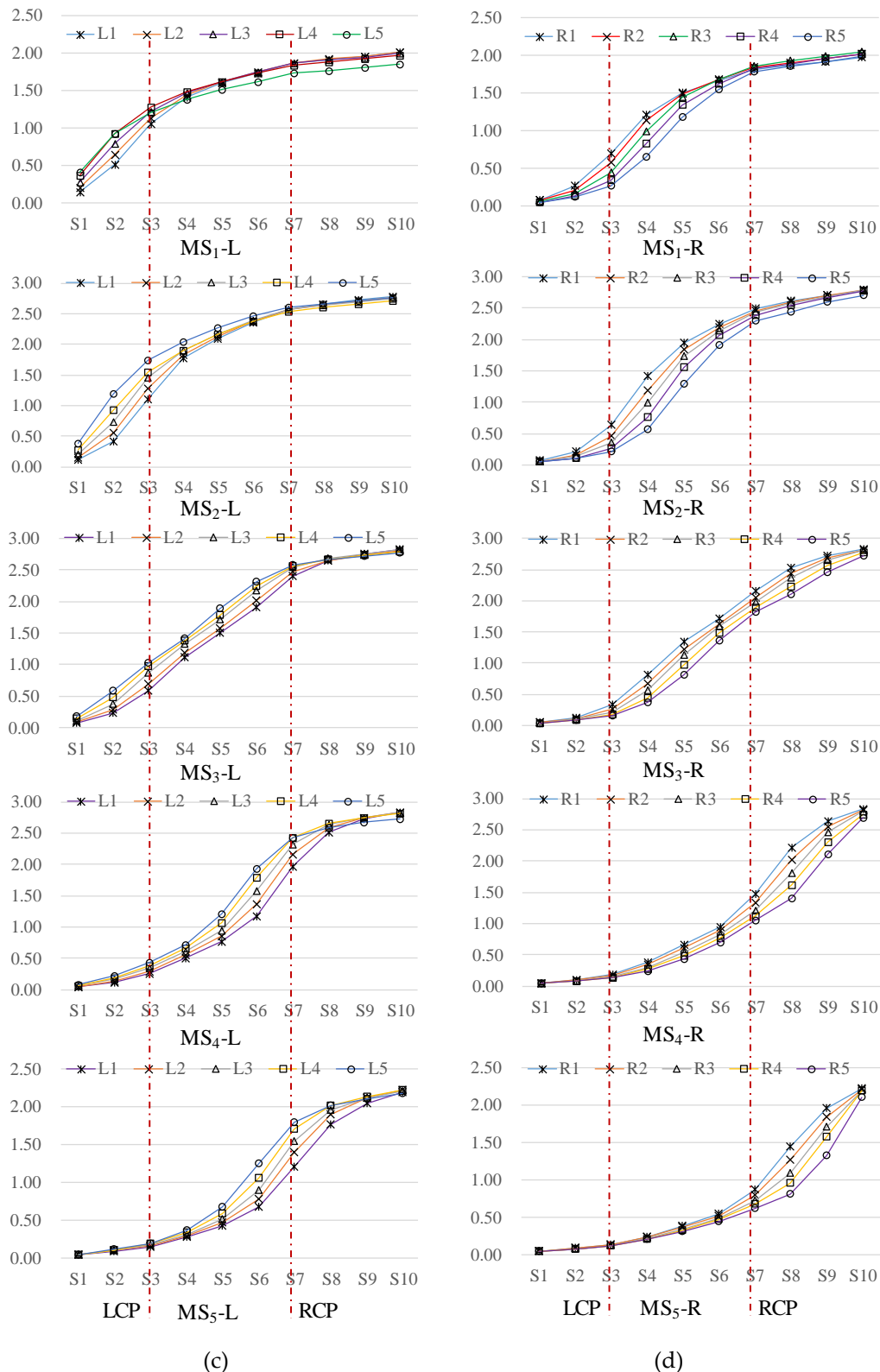
Figure 30 shows the existing tunnel profile measurement point excavation data extraction time step and the total displacement change curve, through the different profile measurement point displacement evolution law is analyzed to obtain the displacement characteristics of the measurement point.
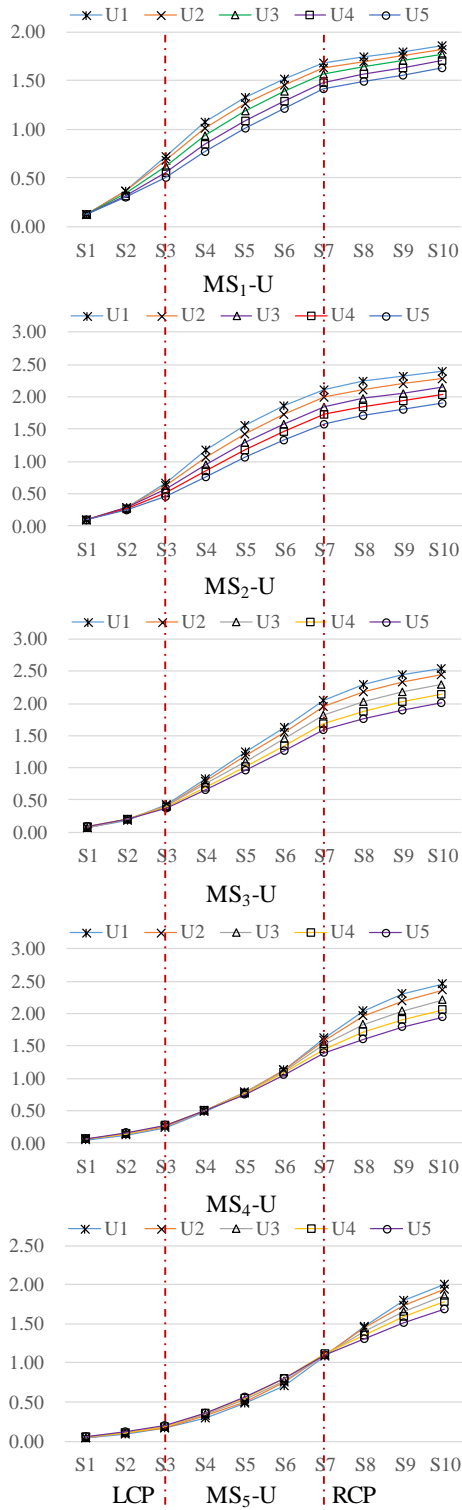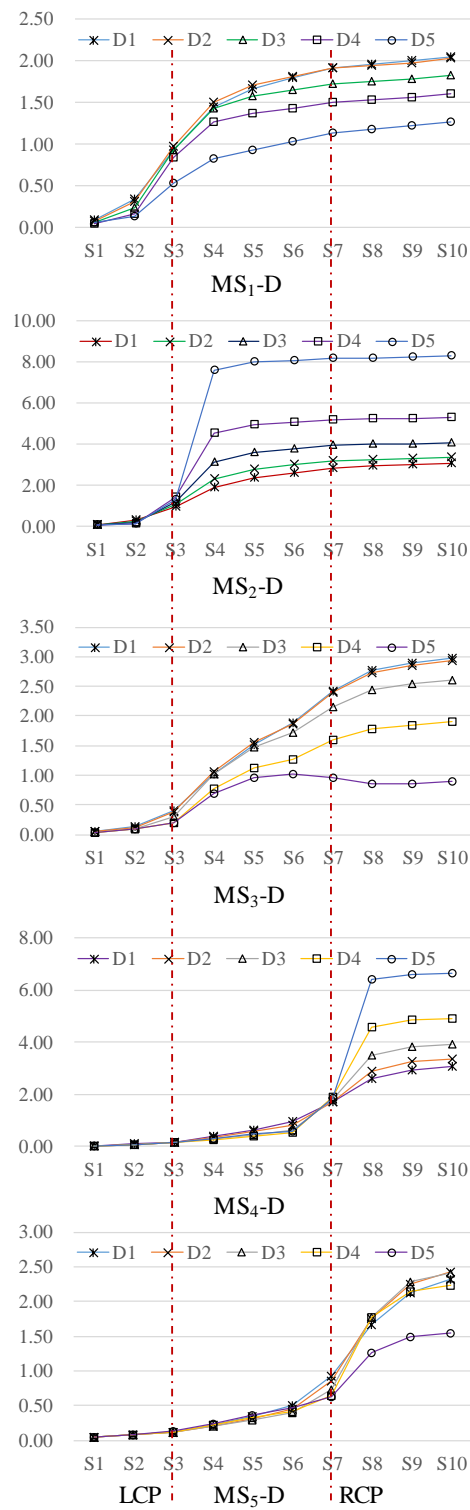
(a)   (b)

Figure 30. Plot of the total displacement change versus the time step when extracting excavation data from typical profiles of existing tunnels: (a) vault; (b) floor; (c) left wall; (d) right wall; the red lines are 12m apart, referring to the distance between L2 and L4.

Vaulting points: The tunnel structure points in the middle profile of the left and right tunnels (MS3) were affected by the two tunnel excavations and had the largest total displacement; followed by the left and right tunnel profiles (MS2 and MS4) with comparable displacement values; and finally by the MS1 and MS5 tunnel structure points, with the MS5 tunnel structure point having a larger

displacement than that of the MS1 point. With the excavation time step (S1 and S2), MS1 and MS2 profile points are the first to produce displacement disturbance, because of the new tunnel and the existing tunnel for the diagonal angle; the left line intersection with the latter time step (S3 and S4) displacement growth slope is the largest, from the tunnel structure measuring point to away from the tunnel body measuring point displacement value gradually decreases, the difference between the measuring points is a trend of growth; S5 ~ S7 excavation process of the displacement value of the measuring points is a trend of growth, slope is a trend of decrease S5~S7 excavation process displacement value of each measuring point shows a growing trend, the slope tends to decrease; after S8 excavation, the slope change tends to stabilize, the difference between the measuring points does not change much.MS3 profile from the left line excavation to the intersection (S3) each measuring point began to produce displacement perturbation; to the right line intersection after the excavation (S4~S7), the slope of the growth of the displacement value of each measuring point remains stable; after that (S8~S10) the displacement value of each measuring point shows a trend of growth, the slope shows a tendency to reduce, and the difference between the measuring points does not change much. In MS4 profile, the displacement difference between measuring points is not obvious during the excavation of the left line (S1~S6), the displacement difference between the right line excavation to the intersection point and the next step (S7 and S8) shows an increasing trend, and after that (S9~S10) the difference does not change much; when affected by the excavation of the left tunnel (S1~S4), the displacement of the measuring points away from the cave body gradually increases, and the value of the difference between the points increases gradually, and the value of the difference between the points increases gradually, and the difference between the points increases gradually. MS5 profile in the left line excavation to the right line excavation to the intersection process (S1 ~ S7) displacement difference between measurement points is not obvious, and then (S8 and S9) displacement difference is increasing; S1 ~ S6 excavation process, the displacement difference between measurement points is not obvious. S1~S6 excavation process, from the tunnel structure measuring point to away from the hole body measuring point displacement value gradually increased, the difference between the measuring points is very small; S8~S9 excavation process, from the tunnel structure measuring point to away from the hole body measuring point displacement value gradually decreased; the right line intersection S7 excavation process for the left and right lines of the tunnel excavation displacement perturbation impact switching time period.

Bottom plate measurement points: left and right tunnel profiles (MS2, MS4) and left and right tunnel intermediate profiles (MS3) have comparable displacement values, which are larger than that of MS5 tunnel structural measurement point, and MS1 tunnel structural measurement point has the smallest displacement value; MS1 profile measurement point generates displacement perturbation after excavation of S2, and the slope of the displacement growth of the left intersection and the latter one step (S3 and S4) has a high value, and the slope of the displacement growth of the various measurement points in the process of excavation from S5 to S7 gradually becomes smaller, and the slope of S8 is gradually reduced, and the slope of S7 is gradually reduced. The slope gradually becomes smaller, after S8 excavation, the displacement slope of each measurement point does not change much, the displacement difference between the measurement points tends to stabilize, the displacement value gradually decreases from the tunnel structure measurement point to the measurement point far away from the cave body, and the displacement values of D1 and D2 measurement points are similar.The MS2 profile measurement point produces a displacement perturbation after the excavation of S3, and the slope of the displacement growth of the left line intersection is the largest at the step of S4 after the left line intersection, and the displacement of the measurement points changes little, the slope of the measurement points changes little, the slope of the measurement points increases little, the slope of the measurement points increases little, the slope of the measurement points changes little, the slope of the measurement points increases little, the slope of the measurement points increases little. The slope change is not big, the displacement difference between the measuring points tends to be stable, the displacement value gradually increases from the tunnel structure measuring point to the measuring point far away from the cave body, and the displacement difference between the measuring points also tends to increase.MS3

profile measuring point produces displacement disturbance after S3 excavation, the displacement growth slope of the left line intersection and the latter one step (S4 and S5) is high; S6 excavation produces displacement disturbance, and the displacement of the D5 measuring point tends to be stable, D1~ D4 measuring points tend to be stable, and the displacement of D5 measuring point tends to be stable. After excavation of S7 and S8, the slope of displacement growth of D1~ D4 measuring points tends to stabilize, and the displacement difference between measuring points does not change much; the displacement value gradually decreases from the measuring point of tunnel structure to the measuring point far away from the cave body, and the displacement values of D1 and D2 measuring points are similar. The displacement difference between the measuring points in the left excavation process (S1~S6) is not obvious, and the displacement value from the tunnel structure measuring point to the measuring point away from the hole body is gradually decreasing; the displacement value of each measuring point is similar after the excavation value intersection, and the slope of the displacement growth of each measuring point is the largest after the excavation of S8, and the slope of the displacement growth of each measuring point tends to be stable after that, and the difference in the displacement value of each measuring point does not change much, and the displacement value of each measuring point gradually increases from the measuring point of tunnel structure to the measuring point away from the hole body. After S7 excavation and support, the displacement of each measuring point is obviously disturbed, and the displacement value of the tunnel structure measuring point becomes the minimum value; after S7 excavation and support, the displacement growth slope of each measuring point is the largest, and the displacement values of D1~D4 are similar; after that (S8~S10), the displacement of the tunnel structure measuring point tends to be stabilized, and the slope of the displacement growth rate of the D1~D4 measuring points decreases.

Left side wall measurement point: MS1 profile measurement point in S2~S3 excavation support after displacement growth slope is high, from the tunnel structure measurement point to away from the hole body measurement point displacement value gradually increased; after (S4~S10) displacement growth slope gradually reduced, L1~L4 measurement point displacement value is similar, greater than the L5 displacement value. MS2 profile measurement point in S2~S4 excavation support after displacement growth slope is high, from the tunnel structure measurement point to away from the hole body measurement point displacement value gradually increased; after (S5~S10) displacement growth slope gradually reduced, after the tunnel through the displacement value of each measurement point does not have much difference. MS3 profile measurement point in the S2~S6 excavation support after displacement growth slope is high, and changes are not much, the difference in the displacement value of the measurement point; stable; then (S7~S10) displacement value is similar, greater than L5 displacement value. The slope of displacement growth in S2~S6 is high and not much change, and the displacement difference between each point is stable; after that (S7~S10), the slope of displacement growth decreases gradually, and the displacement difference between each point is not much difference after tunnel penetration; the slope of displacement growth in S2~S6 shows a trend of increase, and the displacement difference between each point is increasing; after that (S7~S10), the slope of displacement growth decreases gradually, and the displacement difference between each point is not much difference after tunnel penetration; the displacement difference between each point is not much difference in the S2~S7 and S7, and the displacement difference between each point is not much difference. ~After the excavation and support of S7, the slope of displacement growth shows an increasing trend, and the difference in displacement between the measuring points gradually increases; after that (S8~S10), the slope of displacement growth gradually decreases, and there is not much difference in the displacement values of the measuring points after the tunnel has passed through.

Right side wall measurement points: MS1 profile and MS2 profile measurement points in S2~S4 excavation and support after the displacement growth slope shows a growing trend, the displacement difference between the measurement points gradually increases, from the tunnel structure measurement point to away from the tunnel body measurement point displacement value gradually decreases; after that (S5~S10) displacement growth slope gradually decreases, after the

tunnel through the displacement value of the measurement points does not differ. After the excavation and support of S2~S4, the slope of displacement growth shows an increasing trend, and the displacement difference between the measuring points gradually increases; after the excavation and support of S5~S8, the slope of displacement growth remains stable, and the displacement difference between the measuring points does not change much, and the displacement value gradually decreases from the measuring point of the tunnel structure to the point of the measuring point far away from the tunnel body; after that, the slope of displacement growth decreases, and there is not much difference in the displacement value of the measuring points after the tunnel passes through; after the excavation and support of S4, the displacement growth slope decreases, and there is not much difference in the displacement value of the measuring points after the tunnel passes through. After the excavation and support of S8, the slope of displacement growth tends to increase, the displacement difference between the measuring points gradually increases, and the displacement value from the tunnel structure measuring point to the measuring point far away from the cave body gradually decreases; after that (S9 and S10), the slope of displacement growth gradually decreases, and there is not much difference in the displacement value of each measuring point after the tunnel is through. The displacement difference between the measurement points gradually decreases, and the displacement value gradually increases from the tunnel structure measurement point to the measurement point far away from the tunnel body; the displacement growth slope decreases after the excavation of S10, and there is not much difference between the displacement values of the measurement points.

In summary, the displacement of the base plate of the existing tunnel is greatly affected by the excavation time step, and the change rule of the top plate and the left and right side walls is similar. The trend of displacement change at the measuring point is mainly determined by the distance between the excavation surface and the typical profile, and the 40m range in the middle of the tunnel measuring point is the sensitive area affected by the excavation, which shows slow growth when the distance is far away and fast growth when the distance is close.

4.1.2. Von Mises Stress Response

Based on the typical excavation data of the axial section of the new left tunnel and the axial section of the existing tunnel, the Von Mises stress cloud and monitoring point data at different time steps were extracted for mechanical response characterization.

1) Von Mises stress cloud

Figure 31 and Figure 32 show the Von Mises stress maps of the axial section of the new left tunnel and the axial section of the existing tunnel at the typical excavation data extraction time step. After the excavation and support of the new tunnel underneath, the Von Mises stress perturbation area of the excavated tunnel and the new tunnel changes significantly in the support structure, while other areas are slightly perturbed at the initial stage.


S_0 S_3 S_7
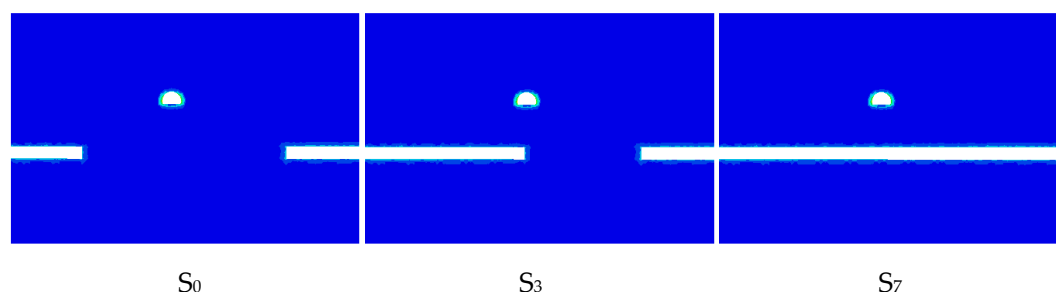
Figure 31. Von Mises stress map of the axial section of the new left tunnel.

S_0 S_4 S_8
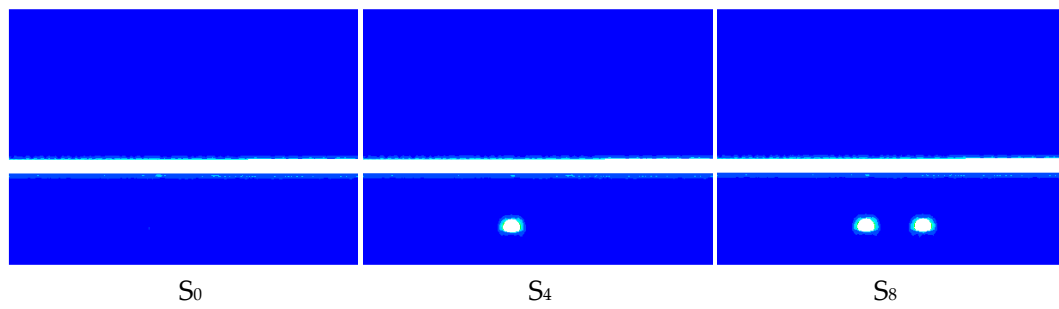
Figure 32. Von Mises stress map of the axial section of the existing tunnel.

2) Monitoring point data

Figure 33 shows the time step of excavation data extraction and Von Mises stress change curves of typical profile measurement points of existing tunnels, and analyzes the Von Mises stress evolution law of different profile measurement points.
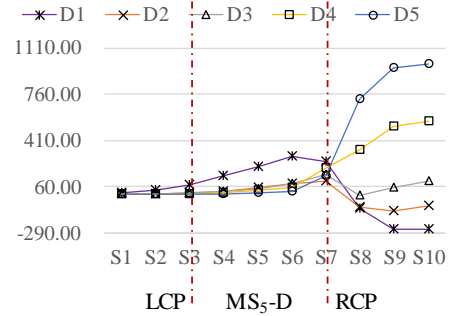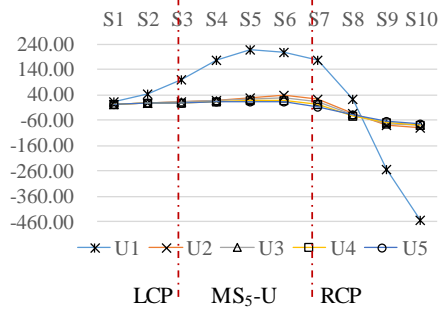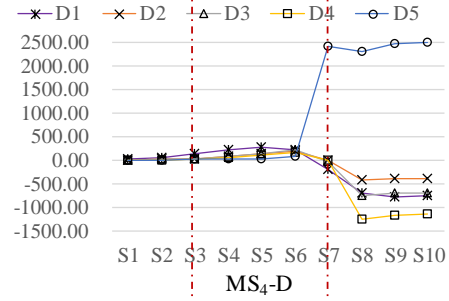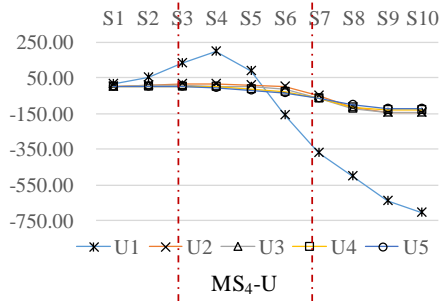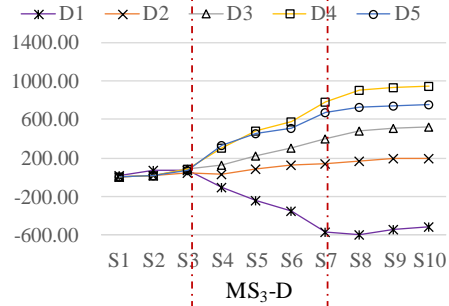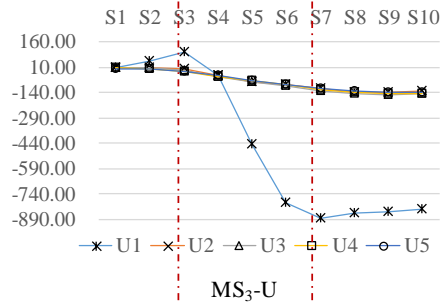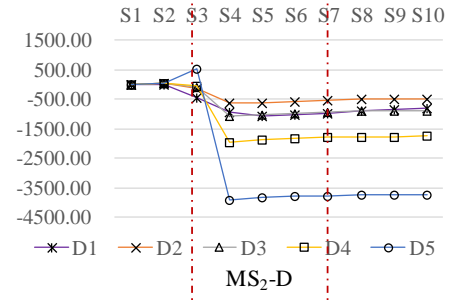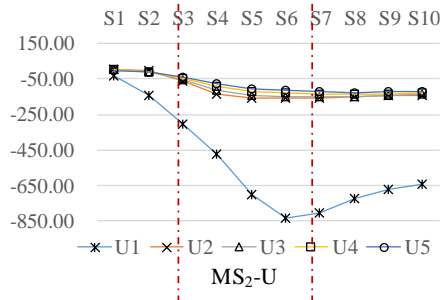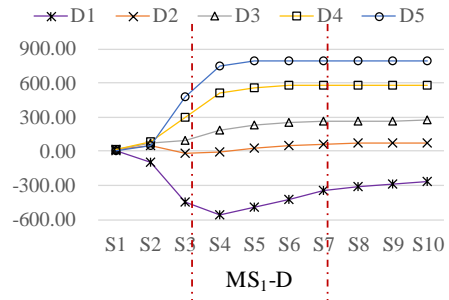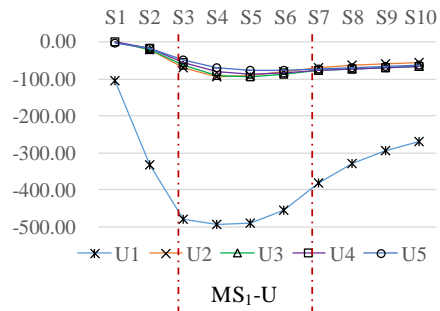
(a)   (b)
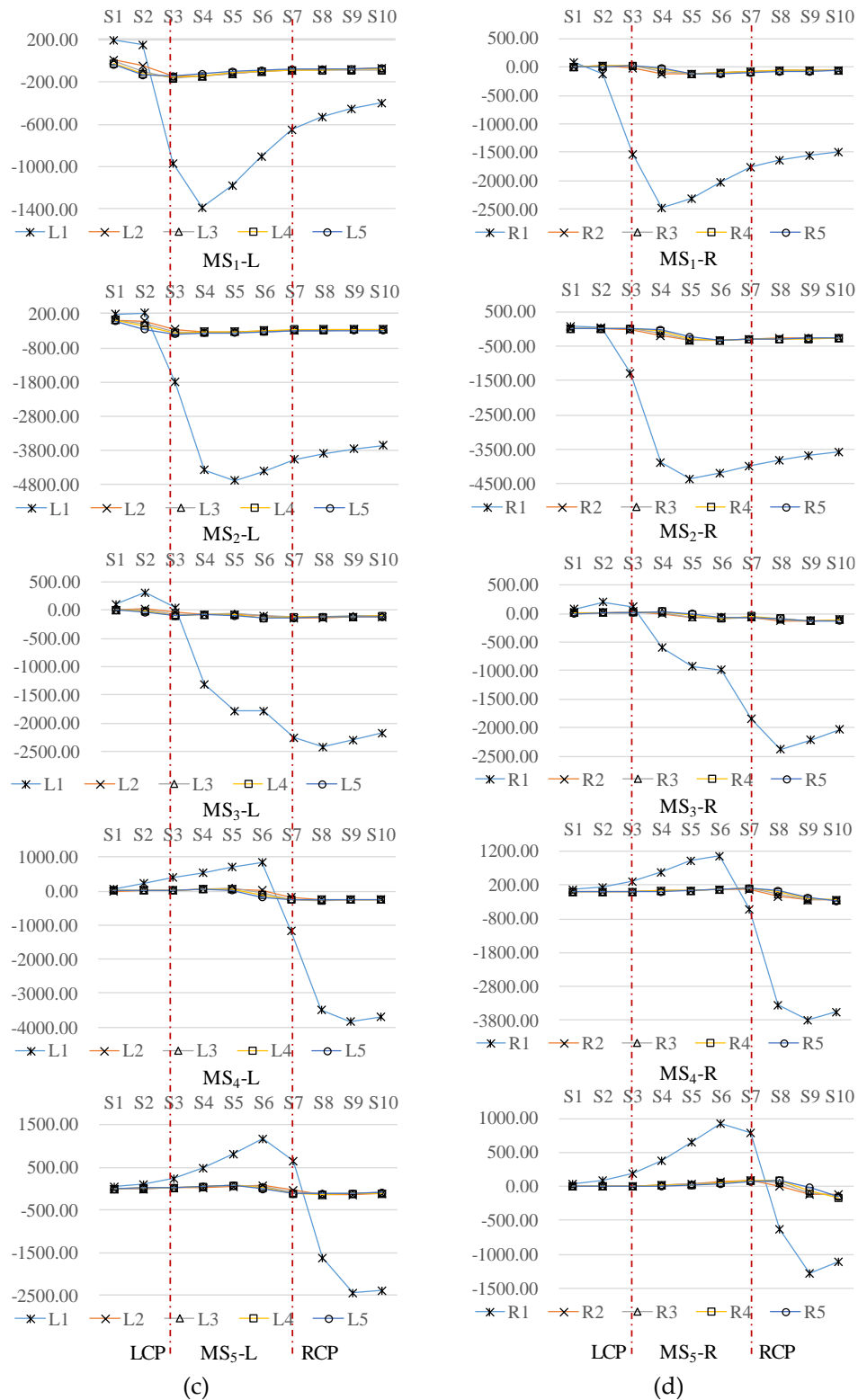
Figure 33. Plots of the time step of excavation data extraction versus Von Mises stress change curves for typical profiles of existing tunnels: (a) arch; (b) floor; (c) left wall; (d) right wall; the red lines are spaced at intervals of 80 m, which refer to the time step of excavation data extraction from S3 to S7.

Vertex measurement points: Von Mises stress changes at the tunnel structure measurement points in MS1~MS5 profiles are prominent, while the values of Von Mises stress changes at the other measurement points are similar. Mises stress changes show two stages of rapid decline (S2~S6) and rebound (S7~S10); MS3 profile U1 measurement point Von Mises stress changes show three stages of slow rise (S2 and S3), rapid decline (S4~S7), and stabilization (S8~S10); MS4 profile U1 measurement

point Von Mises stress changes show three stages of slow rise (S2~S4) and rapid decline (S5~S10); MS5 profile U1 point Von Mises stress change manifested as a slow rise (S2~S5), a slow decline (S6 and S7), a rapid decline (S8~S10) three phases; each profile U2 ~ U5 point Von Mises stress change law is similar to the U1 point, the range of the fluctuation of the stress value is smaller, the change stage is slow. small, the change stage is slow.

Bottom plate measurement points: MS1 profile measurement points can be divided into four categories according to the change rule of Von Mises stress into D1 measurement point stress drop in the strong perturbation region, D2 measurement point stress stable micro-disturbation region, D3 measurement point stress rise in the low perturbation region, D4 and D5 measurement point stress rise in four categories of strong perturbation region; D1 measurement point Von Mises stress change manifested as a slow decline (S2), a rapid decline (S3 and S4), rebound (S4), and a rapid decline (S3 and S4), and a rapid decline (S4).   D4 and D5 points show four stages of Von Mises stress change: slow rise (S2), rapid rise (S3 and S4), slight rise (S5~S7), and stabilization (S8~S10).MS2 profile points can be divided into D1~D3 points according to the change rule of Von Mises stress change into the region of low disturbance, D4 points into the region of medium disturbance, and D5 points into the region of medium disturbance.   According to the change rule of Von Mises stress, the D1 stress can be divided into four categories: D2 stress is stable and slightly disturbed, D3 stress is rising and low disturbed, and D4 and D5 stress is rising and strongly disturbed; the D1 Von Mises stress is in five stages: S2, S3, S4~S7, S8, and S10; the D2 Von Mises stress is in five stages: S5~S7, S8 and S10; and the D2 Von Mises stress is in five stages: S5~S7, S8 and S10. Von Mises stress change at the measurement point exhibits three stages of slightly rising (S2 and S3), slightly falling (S4), and slowly rising (S5~S10); D3 Von Mises stress change at the measurement point exhibits four stages of slightly rising (S2), slowly rising (S3 and S4), rising (S5~ S8), and stabilizing (S9~S10); and D4 and D5 measurement point Von The Von Mises stress changes in the D4 and D5 measurement points can be divided into five stages: slightly rising (S2), slowly rising (S3), rapidly rising (S4), rising (S5~S7), and stabilizing (S8~S10).The MS4 measurement points can be divided into three categories: D1~D3 measurement points with low stress reduction and low perturbation area, D4 measurement points with medium stress reduction and medium perturbation area, and D5 measurement points with strong stress rise and strong perturbation area. D1~D3 measuring point Von Mises stress change manifested as a slight rise (S2~S6), rapid decline (S7 and S8), stable (S9~S10) three stages; D4 measuring point Von Mises stress change manifested as a slight rise (S2~S6), decline (S7), rapid decline (S8), a slight increase in the four stages (S9~S10); Von Mises stress change at D5 measurement point is characterized by five stages: slightly rising (S2~S6), rapidly rising (S7), slightly falling (S8), slightly rising (S9), and stabilizing (S10).MS5 profile measurement points can be divided into D2 and D3 measurement points with low disturbance, D1 and D4 measurement points with medium disturbance, and D5 and D5 measurement points with strong disturbance.   S10) four stages;D4 measuring point Von Mises stress change shows three stages of slight rise (S2~S6), rapid rise (S7~S9), and slight rise (S10); D5 measuring point Von Mises stress change shows four stages of slight rise (S2~S6), rise (S7), rapid rise (S8~S9), and slight rise (S10).

Side wall measurement points: the change rule of Von Mises stress at the measurement points of left and right side wall profiles is consistent, the change of Von Mises stress at the measurement points of tunnel structure is prominent, and the change of Von Mises stress at the other measurement points has similar values. the change of Von Mises stress at the U1 measurement point of the MS1 profile exhibits a slow decline (S2), a rapid decline (S3 and S4), and a rapid rebound (S5~S7), slow recovery (S8~S10), four stages; MS2 profile U1 measurement point Von Mises stress change shows a slow decline (S2), rapid decline (S3 and S4), slow decline (S5), slow recovery (S6~S10) four stages; MS3 profile U1 measurement point Von Mises stress change shows a slow rise (S2), slow decline (S3) MS5 profile U1 Von Mises stress change manifested as a slow rise (S2 ~ S6), slow decline (S7), rapid decline (S8 ~ S9), slow recovery (S10) four stages; each profile U2 ~ U5 measurement point Von Mises stress change law is similar to the U1 measurement point, the range of the stress value floating smaller, the change stage are slow.

Comprehensive analysis concludes that: the existing tunnel roof and side wall point Von Mises stress disturbance mainly occurs in the tunnel structure area. The distance between the excavation surface and the typical profile determines the trend of stress change at the measuring point, which is characterized by stress rise when the distance is far away and stress fall when the distance is close, and can be classified into four types: micro, slow, normal and fast. The sensitive distance of roof stress disturbance ranges from 2 to 4 excavation data extraction time steps, i.e. 40~80m range; the sensitive distance of side wall stress disturbance ranges from 2 to 3 excavation data extraction time steps, i.e. 40~60m range. Existing tunnel floor measuring point Von Mises stress disturbance can be divided into four types: micro, low, medium and high, the tunnel structure measuring point is in the stress reduction in the level of disturbance, the rule of change is similar to the tunnel structure measuring point in other regions; there are pressure relief and pressure-bearing areas in the tunnel floor area, during the excavation process of the left tunnel, the proximity of the measuring point is the pressure relief area of the stress reduction, and the long-distance distance measuring point is the pressure-bearing area of the stress rise. Under the influence of the stress disturbance of the left tunnel excavation, the measuring points far away from the tunnel structure during the excavation of the right tunnel produced the phenomenon of stress rise under pressure, indicating the existence of a pressurized stress arch. The stress disturbance sensitive distance ranges from 1~2 excavation data extraction time steps, i.e. 20~40m range.

4.2. Typical Profile Analysis

Based on the total displacement characteristics of typical profiles and mechanical characteristics of typical measurement points in the affected area under different calculation conditions, and the mechanical characteristics of the existing tunnel floor, the mechanical response characteristics are analyzed, and the construction method is optimized.

4.2.1. Total Displacement Characterization

The total displacement maps (Figure 34) of the axial profile of the existing tunnels at the time of tunnel penetration were extracted for the four calculation conditions to analyze the characteristics of the total displacement of the axial profile.
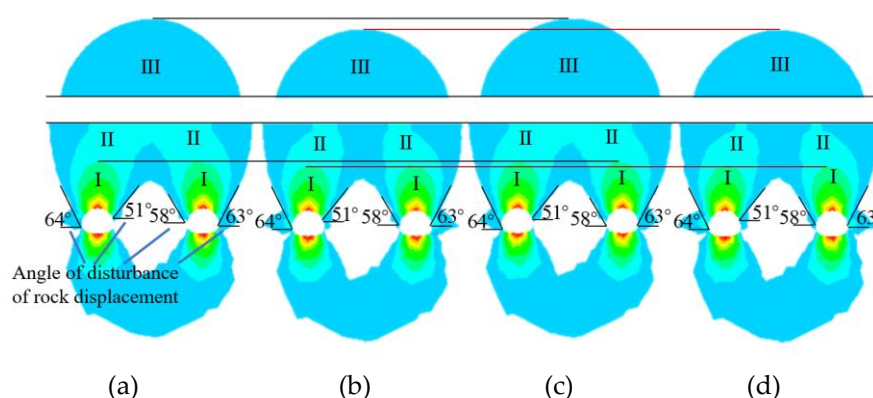
Figure 34. Clouds of the total displacement of the rock formation under different calculation conditions: (a) UPBM; (b) UPSM; (c) CDBM; (d) CDSM.

The total displacement of the rock layer in the profile of the existing tunnel is basically the same under the four calculation conditions: the strong disturbance region III and the low disturbance region I of the UPBM and CDBM methods are of the same height, and the middle disturbance region II is connected at double the diameter of the existing tunnel; the strong disturbance region I and the low displacement disturbance III of the UPSM and CDSM methods are of the same height, which is a little lower than the height of the excavation of the blast method, and the middle disturbance region of displacement II is not connected.

4.2.2. Typical Point Characteristics

Comparison and analysis of the total displacement and Von Mises stress extremes of existing tunnel measurement points in typical profiles for the four calculation conditions.

1) Analysis of total displacement at measuring points
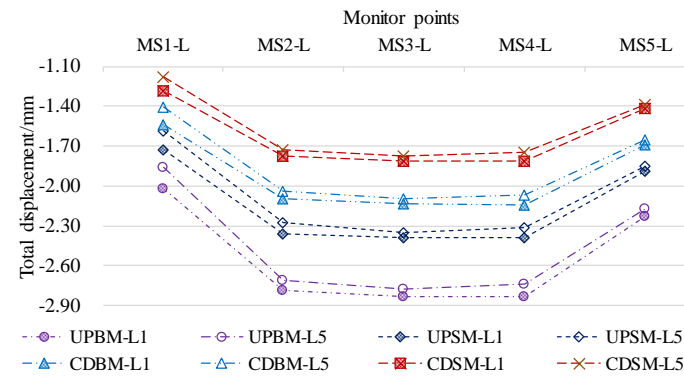
Figure 35 shows the comparison curves of the total displacement at the typical profile of existing tunnels under different working conditions.
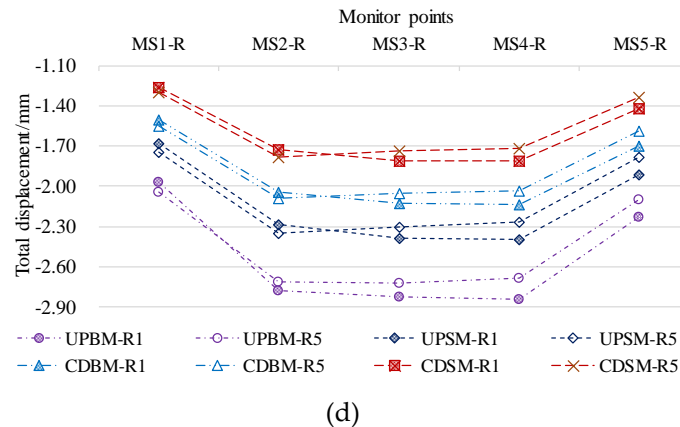

(a)

(b)

(c)

(d)
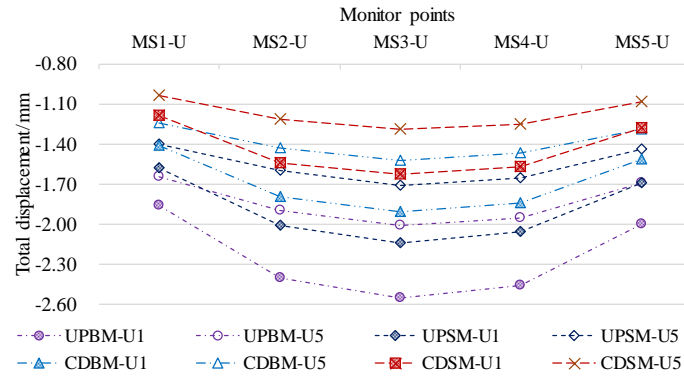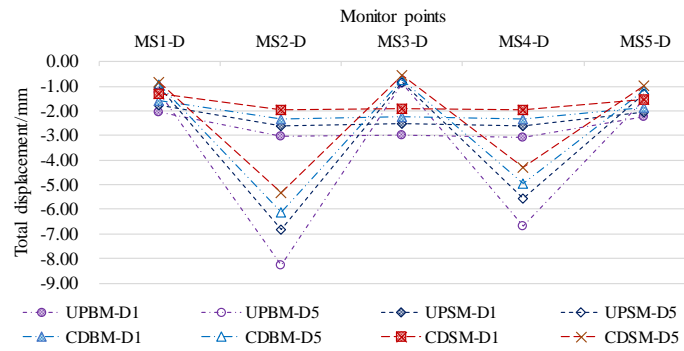
Figure 35. Comparison curves of total displacement extremes of typical profiles of existing tunnels with different working conditions: (a) arch top; (b) floor; (c) left wall; (d) right wall.

The total displacement change rule of measuring points in MS1~MS5 profiles of the tunnel under the four calculation conditions is the same, and the extreme value of the typical measuring points of the upper and lower step blasting method excavation is the largest, followed by the upper and lower step static method, CD blasting method and CD static method.

The total displacement of the arch measuring points U1 and U5 in the MS3 profile is the largest, and the values of both profiles decrease symmetrically, and the settlement value of measuring point U1 is larger than the settlement value of measuring point U5. Upper and lower step blasting method excavation measuring point U1 and U5 total displacement extreme value of 2.55mm and 2.01mm.

The total displacement extreme value of measuring point D1 of the base plate tunnel structure is obvious in MS2~MS4 profile settlement, with similar values, MS4-U1 is larger than MS2-U1 is larger than MS3-U1. The total displacement extreme value of measuring point D5 of the base plate away from the tunnel structure is prominent in MS2 and MS4 profile settlement, with MS2-U5 > MS4-U5, and the total displacement extreme value of measuring point D5 of the MS1, MS3, and MS5 profiles are smaller, with similar values. The values are similar. The extreme values of total displacement of measuring points U1 and U5 in the excavation of upper and lower step blasting method are 3.09mm and 8.27mm.

Typical measurement points of the left and right side walls have similar total displacement extremes, and the settlement is obvious in the MS2~MS4 profile, with similar values. The total displacement extremes of measuring points L1 and L5 of the upper and lower step blasting method excavation are 2.83mm and 2.78mm; the total displacement extremes of measuring points R1 and R5 are 2.84mm and 2.72mm.

2) Von Mises stress analysis at measurement points

Figure 36 shows the comparison curves of Von Mises stress extremes at typical profile measurement points for existing tunnels with different operating conditions.
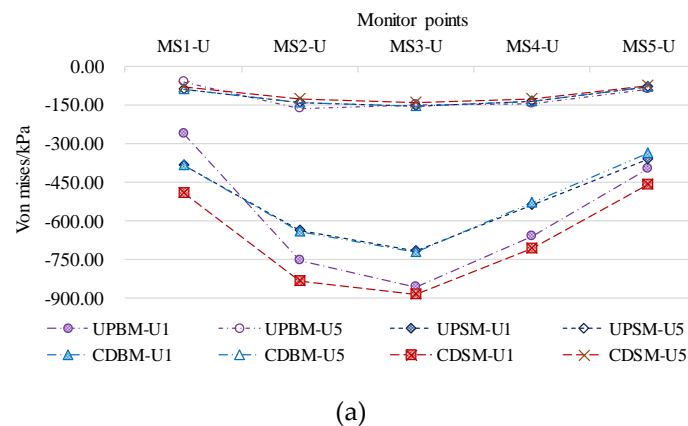
(a)
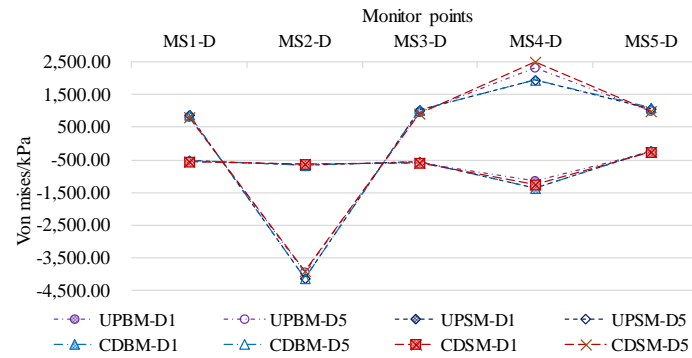
(b)

(c)

(d).

Figure 36. Comparison curves of Von Mises stress extremes at typical profile measurement points of existing tunnels with different working conditions: (a) arch; (b) base plate; (c) left wall; (d) right wall.

The Von Mises stress extremes of the tunnel structure measurement points and the farthest end measurement points in the four calculation conditions MS1~MS5 profiles have similar patterns.

The Von Mises stress increase values of the arch measuring point U1 are all negative increase, and the negative increase value of MS3 profile is the largest; 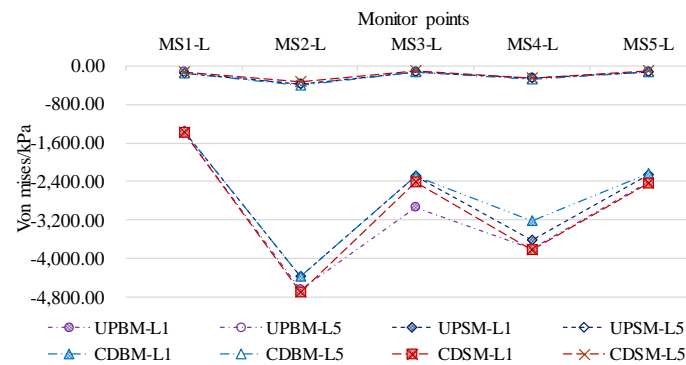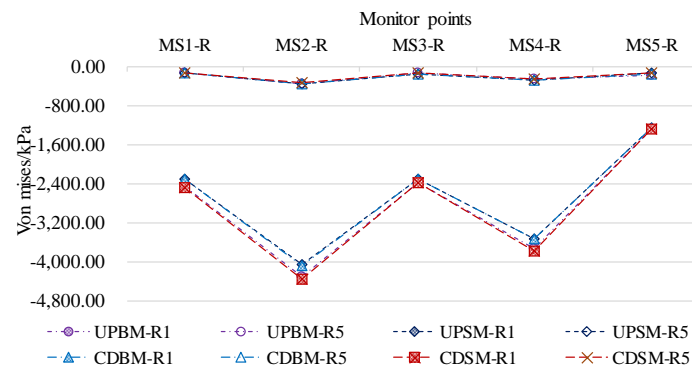the values of the upper and lower step blasting method and CD static method are similar, and the difference between the upper and lower step static method and CD blasting method is not much; the negative change extreme value of the Von Mises stress of the measuring point U5 of the CD static method is the largest and it is -887.42kPa; the Von Mises stress increase values of the arch measuring point U5 are all negative increase, and the negative change extreme value is -887.42kPa. Von Mises stress increase value are negative increase, the change value is small, and the values of different calculation conditions are similar, and the distribution of Von Mises stress negative change extreme value is from -139.74 to -164.41 kPa.

The Von Mises stress increase values of the bottom plate measurement point U1 are all negatively increasing, and the negative increase value of the measurement point in MS4 profile is the

largest, and the values of the measurement points of the four working conditions have similar amount of change; the negative change extreme value of the Von Mises stress of the measurement point of the excavation by CD blasting method is the largest, and it is -1634.97 kPa.The negative change extreme value of the Von Mises stress of the measurement point U5 is negatively increasing in the MS2 profile, and it is -139.74 ~ -164.41 kPa in the MS1, MS3, MS4 and MS5 profiles are negatively increased, and positively increased in MS1, MS4 and MS5 profiles, and the values of the four working conditions are similar; the negative value of the Von Mises stress at the upper and lower step static method excavation point U5 is the largest, which is -4150.37kPa; the positive value of the Von Mises stress at the CD static method excavation point U5 is the largest, which is 2496.89kPa.

The extreme value of Von Mises stress at the left and right sidewall tunnel structure measurement points is similar in different calculation conditions, the negative change of the measurement point value in MS2 and MS4 profile is prominent, and the negative change of the measurement point value in MS2 profile is the largest; the extreme value of the measurement point in CD static method excavation is the largest, the extreme value of the measurement point L1 is -4696.90 kPa, and the extreme value of the measurement point R1 is -4366.50 kPa. different calculation conditions of the left and right sidewalls The extreme value of Von Mises stress at the measurement point far away from the tunnel structure is similar, the extreme value of negative change at the measurement point of MS2 profile is the largest, and the extreme value of the measurement point of CD blasting method is the largest; the extreme value of the measurement point L5 is -398.64 kPa, and the extreme value of the measurement point R5 is -360.02 kPa.

### 4.2.3. Characterization of Bottom Plate Measurement Points

Based on the data of total displacement, Von Mises stress, high and low tilt values of the centerline of the bottom plate of the step tunnel at the time of tunnel penetration under different excavation methods, the control effect on the mechanical response of the bottom plate of the existing tunnel is analyzed.

Figure 37 shows the total displacement and settlement curves of the existing tunnel base plate under different excavation methods, which shows that the total displacement and settlement of the existing tunnel base plate under different excavation methods are consistent. Taking the centerline of the left and right tunnels as the axis, the data of the left and right measurement points are symmetrically distributed, and the value of the right measurement point is slightly larger than the value of the left measurement point, which is mainly due to the fact that the left tunnel is the first one to be excavated, which is caused by the spatial mechanical effect. The settlement value of the area between the intersection points of the left and right tunnels is the largest, and the settlement value gradually decreases to both sides, and after a certain distance, it is an overall uniform settlement area. In the area between the intersection points, the displacement settlement order is as follows: upper and lower step blasting method excavation settlement value of up to 3.09mm, upper and lower step static method excavation settlement value of up to 2.64mm, CD blasting method excavation settlement value of up to 2.35mm, CD static method excavation settlement value of up to 1.97mm; outside the intersection point of the left side of the region, upper and lower step blasting method, upper and lower step static method, CD The left area outside the intersection point, the upper and lower step blasting method, upper and lower step blasting method, CD static method excavation settlement value is similar, greater than the CD static method excavation settlement value; outside the intersection point of the right area, the upper and lower step blasting method, CD blasting method excavation, CD static method excavation settlement value is similar, less than the upper and lower step blasting method excavation settlement value. Locate the settlement sensitive area between measurement points 6 and 16, the distance is 130m.
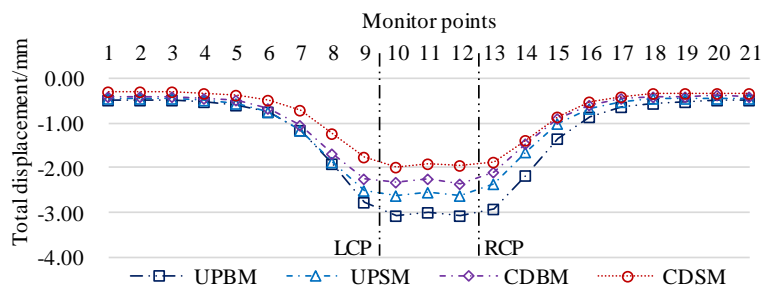
Figure 37. Total displacement and settlement curve of the base plate of existing tunnels with different methods of excavation.

Figure 38 shows the change curve of Von Mises stress in the centerline of the existing tunnel base plate after different excavation methods are adopted for the new tunnel, and the change rule is consistent. Taking the left and right tunnel centerline as the axis, the data of left and right measurement points are symmetrically distributed, and the values of Von Mises stress change in the middle line of the base plate of existing tunnels under the four excavation methods are similar. Left and right intersection area Von Mises stress negative change is the largest, for the high decompression area, the upper and lower step blasting method excavation maximum negative change to -669kN, the upper and lower step static method excavation maximum negative change to -591kN, the CD blasting method excavation maximum negative change to -593kN, the CD static method excavation maximum negative change to -683kN; the center of the lower tunnel link is medium decompression area, the negative change of the stress is Decrease; to the intersection of the left and right sides of the Von Mises stress negative change gradually become smaller to positive change from the pressure relief area and turn into a pressurized area, measurement points 6, 7 and 15, 16 for the higher pressurized area, up and down the steps of blasting method of excavation of the largest positive change to 236kN, up and down the steps of static method of excavation of the largest negative change to 199kN, CD blasting method of excavation of the largest negative change to 199kN, CD static method of excavation of the largest The maximum negative change is 243kN; on both sides of the higher pressure-bearing area, the positive change of Von Mises stress gradually decreases, and the transition from the high pressure-bearing area to the slightly disturbed area. The sensitive area of Von Mises stress change is located between measurement points 6 and 16, with a distance of 130m.
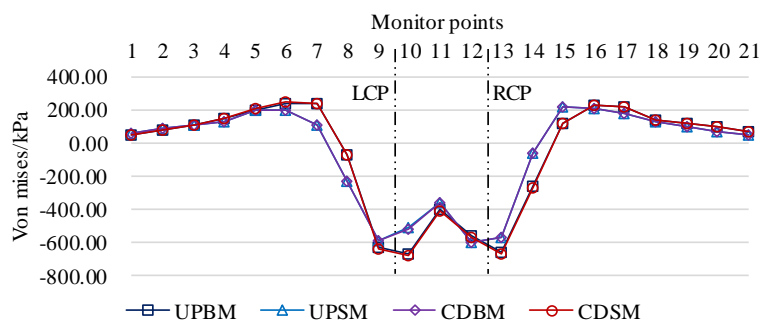
Figure 38. Von Mises stress curve of existing tunnel base plate with different excavation methods.

Figure 39 shows the curve of high and low inclination values of the centerline of the base plate of the existing tunnel under different excavation methods, and the high and low inclination values of the base plate are calculated by Equation (12) [38]:

$$f = [\delta] \,/\, L \tag{12}$$

Where, f is the value of the height and tilt of the base plate, $[\delta]$ is the maximum vector difference between neighboring measurement points of the base plate, L is the distance between neighboring measurement points
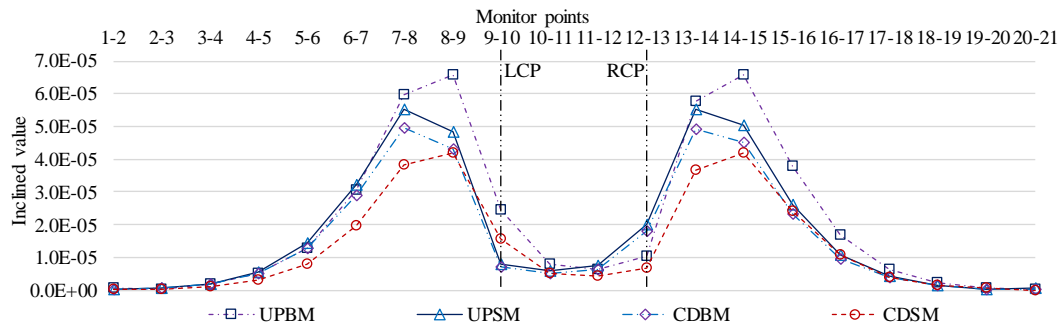
Figure 39. Variation of the base plate height and inclination values of existing tunnels with different excavation methods.

According to the total displacement settlement value of the existing tunnel base plate under different excavation methods, calculated by formula (12) (L takes 13m), the curve of high and low tilt value of the centerline of the existing tunnel base plate under different excavation methods is derived. Taking the centerline of the left and right tunnels as the axis, the data of the left and right measurement points are approximately symmetrically distributed, and their change rules are similar, and they are in order from the end to the axis: micro-growth, growth, rapid growth, rapid decline, decline in five stages. The intersection of the left and right tunnels to the higher pressure-bearing area is the sensitive area for the change of high and low tilt values, i.e., measurement points 6-7, 7-8, 8-9 and measurement points 13-14, 14-15, 15-16 area. In the areas sensitive to changes in high and low tilt values, the tilt values in order of magnitude are as follows: the maximum tilt value of the upper and lower step blasting method excavation is $6.57×10^{-5}$, the maximum tilt value of the upper and lower step static method excavation is $5.54×10^{-5}$, the maximum tilt value of the CD blasting method excavation is $4.94×10^{-5}$, and the maximum tilt value of the CD static method excavation is $4.30×10^{-5}$.

4.2.4. Excavation Method Preference

The Von Mises stress changes in the base plate of the existing tunnel caused by the four underpass tunnel excavation methods are small and similar, and the existing tunnel structure is in a safe condition. Therefore, in this paper, the excavation methods are preferred by displacement control criteria[39]. Line static geometry allowable deviation management value, select the high and low tilt value as the evaluation index, the allowable management value is shown in Table 5.

Table 5. Table of permissible values for high and low inclination of railway tracks.

Train speed	Operational acceptance	Regular maintenance	Temporary repairs
200~250km/h	0.0002	0.0005	0.0008
250~300km/h	0.0002	0.0004	0.0007

Assuming that the tilt value of the base plate and the tilt value of the railway track are equal, the operation acceptance tolerance value is selected as the high and low tilt value tolerance value, i.e., 0.0002. After excavation of the four methods, the tilt value of the base plate of the existing tunnel ranges from 6.57×10-5 to 4.30×10-5, which is less than the evaluation tolerance value, and it meets the displacement and deformation control standard. Combined with the construction efficiency and cost[31], the upper and lower step blasting method is preferred and recommended for excavation. During the construction process, monitoring and measurement are strictly implemented, and 70% of the permissible value is set as the warning threshold, and when the warning threshold is reached, the excavation should be adjusted to CD blasting method in time.

5. Conclusions

This paper investigates the excavation mechanical characteristics of a double-line highway tunnel under the influence of dynamic and static loads with oblique angle under the railway tunnel. Through the method of photographic images and over-advanced geological forecast information, the rock parameters in the influence area of the cross-tunnel project under dynamic and static loads are determined by using the quantitative method of disturbance system and Hoek-Brown criterion, and the engineering scale model of the mechanical excavation of the tunnel under the underpass and the four kinds of calculation conditions are constructed, and the mechanical characteristics of the double-line highway tunnel under the influence of dynamic and static loads are revealed on the basis of the analysis of the data of the rock layers in the influence area and mechanical characteristics of the typical section. Mechanical response mechanism of excavation under dynamic and static loads of double-line highway tunnels under the influence of existing railway tunnels is revealed.

(1) The rock layer movement law of the new tunnel is that the upper rock layer moves downward, the bottom rock layer moves upward, the arch of the tunnel structure sinks, the bottom plate bulges, and the sidewalls move outward; the rock layer displacement influence area of the upper and lower parts of the new tunnel includes four areas, namely, the strong disturbance area I, the medium disturbance area II, the low disturbance area III, and the micro-disturbance area IV. Sidewall rock displacement impact area is mainly for the low disturbance region III, micro-disturbance region IV two regions, the impact area is arch-shaped, with the increase in tunnel excavation and support length of the tunnel on the upper and lower tunnel arch height and width of the increasing trend; left tunnel and right tunnel excavation and support process of the strong disturbance region and the disturbance region of the law of change is similar to the expansion of the region alone. The low-disturbance zone and the micro-disturbance zone are synergistically expanded on the basis of the first excavation of the affected area. In the middle area of the left and right tunnels, there are micro-disturbed and undisturbed areas.

(2) The displacement of the bottom plate of the existing tunnel is greatly affected by the excavation time step, and the change rule of the top plate and the left and right side walls is similar. The displacement trend of the measurement point is mainly determined by the distance between the excavation surface and the typical profile, and the 40m range in the middle of the tunnel measurement point is the sensitive area affected by the excavation, which shows slow growth when the distance is far away and fast growth when the distance is close.

(3) The rock disturbance angle and displacement change rule of new tunnels under four calculation conditions are basically the same: UPBM and CDBM methods have the same height of displacement III strong disturbance region arch and I low disturbance arch, and the displacement II medium disturbance region is connected at double the diameter of the existing tunnel under the base plate; the two static excavation methods have the same height of displacement I strong disturbance region arch and III low displacement arch, which is a little lower than the height of excavation of the blast method, and the displacement II medium displacement arch is slightly lower than the height of excavation of the blasting method. excavation height, displacement II in the disturbed area is not connected.

(4) Von Mises stress disturbance of the roof and side walls of the existing tunnel can be divided into four types: micro, slow, normal and fast, which mainly occur in the tunnel structure. The spatial distance between the excavation surface and the existing tunnel determines the trend of stress change at the corresponding location, which is manifested as stress rise when the distance is far away and stress fall when the distance is close, and the stress change tends to stabilize after a certain distance. The sensitive distance of stress disturbance of roof plate is 40~80m; the sensitive distance of stress disturbance of side wall is 40~60m.

(5) Von Mises stress disturbance of the tunnel floor can be divided into four types: micro, low, medium and high. There are pressure relief zone and pressure-bearing zone in the tunnel floor area. During the excavation of the left tunnel, the area close to the excavation surface is the pressure relief zone with reduced stress, and the far distance is the pressure-bearing zone with increased stress. Affected by the left tunnel excavation stress disturbance, the right tunnel excavation away from the

40

tunnel structure in the area of stress rise pressure phenomenon, the existence of pressure bearing stress arch; stress disturbance sensitive distance of 20~40m.

(6) Extract the total displacement, Von Mises stress, high and low tilt values of the center line of the tunnel floor in different excavation methods when the tunnel passes through, analyze the effect of controlling the mechanical response of the floor of the existing tunnel, compare the excavation methods based on the displacement control criteria, and recommend the up and down step blasting method of excavation.

Author Contributions: Methodology, Y.L.; Formal analysis, Y.L., C.H. and H.L.; Resources, C.H.; Data; curation, C.H., H.L. and C.M.; Writing—original draft, C.H., H.L. and C.M.; Writing—review & editing, H.L. and C.M.; Visualization, C.H., H.L. and C.M.; Funding acquisition, Y.L. All authors have read and agreed to the published version of the manuscript.

Institutional Review Board Statement: Not applicable.

Informed Consent Statement: Not applicable.

Data Availability Statement: Data sharing is not applicale.

Conflicts of Interest: The authours declare no conflict of interest.

References

1. CHEN Y L, CHEN Z L, GUO D J, et al. Underground space use of urban built-up areas in the central city of Nanjing: Insight based on a dynamic population distribution [J]. Underground Space, 2022, 7(5): 748-66.
2. PENG F L, QIAO Y K, SABRI S, et al. A collaborative approach for urban underground space development toward sustainable development goals: Critical dimensions and future directions [J]. Frontiers of Structural and Civil Engineering, 2021, 15(1): 20-45.
3. CHENG H Z, CHEN R P, WU H N, et al. General solutions for the longitudinal deformation of shield tunnels with multiple discontinuities in strata [J]. Tunnelling and Underground Space Technology, 2021, 107.
4. CHEN R P, SONG X, MENG F Y, et al. Analytical approach to predict tunneling-induced subsurface settlement in sand considering soil arching effect [J]. Computers and Geotechnics, 2022, 141.
5. LIU T, XIE Y, FENG Z H, et al. Better understanding the failure modes of tunnels excavated in the boulder-cobble mixed strata by distinct element method [J]. Engineering Failure Analysis, 2020, 116.
6. LI S B, ZHANG Y G, CAO M Y, et al. Study on Excavation Sequence of Pilot Tunnels for a Rectangular Tunnel Using Numerical Simulation and Field Monitoring Method [J]. Rock Mechanics and Rock Engineering, 2022, 55(6): 3507-23.
7. QIU J L, LU Y Q, LAI J X, et al. Failure behavior investigation of loess metro tunnel under local-high-pressure water environment [J]. Engineering Failure Analysis, 2020, 115.
8. ZHAO C Y, LEI M F, SHI C H, et al. Function mechanism and analytical method of a double layer pre-support system for tunnel underneath passing a large-scale underground pipe gallery in water-rich sandy strata: A case study [J]. Tunnelling and Underground Space Technology, 2021, 115.
9. CHAIPANNA P, JONGPRADIST P. 3D response analysis of a shield tunnel segmental lining during construction and a parametric study using the ground-spring model [J]. Tunnelling and Underground Space Technology, 2019, 90: 369-82.
10. LIU B, ZHANG D W, YANG C, et al. Long-term performance of metro tunnels induced by adjacent large deep excavation and protective measures in Nanjing silty clay [J]. Tunnelling and Underground Space Technology, 2020, 95.
11. ZHANG D M, XIE X C, LI Z L, et al. Simplified analysis method for predicting the influence of deep excavation on existing tunnels [J]. Computers and Geotechnics, 2020, 121.
12. DENG Z Y, LIU X R, ZHOU X H, et al. Field monitoring of mechanical parameters of deep-buried jacketed-pipes in rock: Guanjingkou water control project [J]. Tunnelling and Underground Space Technology, 2022, 125.
13. MA J F, HE S H, CUI G Y, et al. Construction stability and reinforcement technology for the super-large rectangular pipe-jacking tunnel passing beneath the operational high-speed railway in composite stratum [J]. Geomatics Natural Hazards & Risk, 2023, 14(1).

14.   MA P, SHIMADA H, SASAOKA T, et al. Investigation on the engineering effects of the geometrical configuration of the jacking rectangular pipe [J]. Tunnelling and Underground Space Technology, 2022, 119.

15.   CHEN F Y, WANG L, ZHANG W G. Reliability assessment on stability of tunnelling perpendicularly beneath an existing tunnel considering spatial variabilities of rock mass properties [J]. Tunnelling and Underground Space Technology, 2019, 88: 276-89.

16.   LIN X T, CHEN R P, WU H N, et al. Deformation behaviors of existing tunnels caused by shield tunneling undercrossing with oblique angle [J]. Tunnelling and Underground Space Technology, 2019, 89: 78-90.

17.   CHEN R P, ZHANG P, WU H N, et al. Prediction of shield tunneling-induced ground settlement using machine learning techniques [J]. Frontiers of Structural and Civil Engineering, 2019, 13(6): 1363-78.

18.   ZHANG P, WU H N, CHEN R P, et al. A critical evaluation of machine learning and deep learning in shield-ground interaction prediction [J]. Tunnelling and Underground Space Technology, 2020, 106.

19.   ZHANG P. A novel feature selection method based on global sensitivity analysis with application in machine learning-based prediction model [J]. Applied Soft Computing, 2019, 85.

20.   ZHOU J, SHI X Z, DU K, et al. Feasibility of Random-Forest Approach for Prediction of Ground Settlements Induced by the Construction of a Shield-Driven Tunnel [J]. International Journal of Geomechanics, 2017, 17(6).

21.   CHEN R P, LIN X T, KANG X, et al. Deformation and stress characteristics of existing twin tunnels induced by close-distance EPBS under-crossing [J]. Tunnelling and Underground Space Technology, 2018, 82: 468-81.

22.   LAI H P, ZHENG H W, CHEN R, et al. Settlement behaviors of existing tunnel caused by obliquely under-crossing shield tunneling in close proximity with small intersection angle [J]. Tunnelling and Underground Space Technology, 2020, 97.

23.   LEI H Y, LIU Y N, HU Y, et al. Active stability of the shield tunneling face crossing an adjacent existing tunnel: transparent clay model test and DEM simulation [J]. Canadian Geotechnical Journal, 2023, 60(6): 864-84.

24.   CHENG R S, CHEN W S, HAO H, et al. A state-of-the-art review of road tunnel subjected to blast loads [J]. Tunnelling and Underground Space Technology, 2021, 112.

25.   TIAN X X, SONG Z P, WANG J B. Study on the propagation law of tunnel blasting vibration in stratum and blasting vibration reduction technology [J]. Soil Dynamics and Earthquake Engineering, 2019, 126.

26.   DUAN B F, GONG W Z, TA G S, et al. Influence of Small, Clear Distance Cross-Tunnel Blasting Excavation on Existing Tunnel below [J]. Advances in Civil Engineering, 2019, 2019.

27.   WU B, CUI Y Z, MENG G W, et al. Research on Dynamic Response of Shallow Buried Tunnel Lining Constructed by Drilling and Blasting Method [J]. Advances in Materials Science and Engineering, 2022, 2022.

28.   RUAN J B, WANG T H, ZHAO Z K, et al. Discussion on Blasting Vibration Velocity of Deep Rock Mass Considering Thickness of Overlying Soil Layer [J]. Periodica Polytechnica-Civil Engineering, 2023.

29.   TIANBIN L I, LUBO M, JIN Z H U, et al. COMPREHENSIVE ANALYSIS METHOD FOR ADVANCED FORECAST OF GEOLOGY IN TUNNELS [J]. Chinese Journal of Rock Mechanics and Engineering, 2009, 28(12): 2429-36.

30.   ZHOU Y, ZHANG B, GENG Z, et al. STABILITY ANALYSIS OF SOFT ROCK SURROUNDING TUNNEL BASED ON HOEK-BROWN STRENGTH CRITERION [J]. Journal of Engineering Geology, 2019, 27(5): 980-8.

31.   GENG Z, ZHANG B, LI W, et al. COMPARISON AND ANALYSIS ON SURROUNDING ROCK STABILITY OF BIAS LARGE SPAN TUNNEL WITH DIFFERENT EXCAVATION METHODS [J]. Journal of Engineering Geology, 2018, 26(4): 866-73.

32.   HU W, LIU J, PANG Y, et al. CORRECTION OF STRENGTH PARAMETERS FOR ANISOTROPIC SLOPE ROCK MASS BASED ON H-B PRINCIPLES [J]. Journal of Engineering Geology, 2018, 26(5): 1196-202.

33.   LI S, LIU B, SUN H, et al. STATE OF ART AND TRENDS OF ADVANCED GEOLOGICAL PREDICTION IN TUNNEL CONSTRUCTION [J]. Chinese Journal of Rock Mechanics and Engineering, 2014, 33(6): 1090-113.

34.   LI Y F, HUANG C F, LU H J, et al. Investigation of the Influence Area of the Excavation of a Double-Line Highway Tunnel under an Existing Railway Tunnel [J]. Applied Sciences-Basel, 2024, 14(1).

35.   MARINOS P, MARINOS V, HOEK E. Geological Strength Index (GSI). A characterization tool for assessing engineering properties for rock masses; proceedings of the Underground Works under Special Conditions Workshop, Lisbon, PORTUGAL, F Jul 06, 2007 [C]. 2007.

36.   HOEK E, BROWN E T. The Hoek-Brown failure criterion and GSI - 2018 edition [J]. Journal of Rock Mechanics and Geotechnical Engineering, 2019, 11(3): 445-63.

37. HEPING X I E, YANG J U, LIYUN L I, et al. ENERGY MECHANISM OF DEFORMATION AND FAILURE OF ROCK MASSES [J]. Chinese Journal of Rock Mechanics and Engineering, 2008, 27(9): 1729-40.

38. WANG Y, YIN J M, XIAO G Q. Three-dimensional stability analysis of stratified rock mass tunnel based on anisotropic theory; proceedings of the 5th International Symposium on In-Situ Rock Stress, Beijing, PEOPLES R CHINA, F Aug 25-27, 2010 [C]. 2010.

39. GUO F, LIU J X, LI Y F, et al. Fatigue life evaluation of high-speed maglev train bogie under higher operating speed grade; proceedings of the 5th International Conference on Transportation Information and Safety (ICTIS), Liverpool, ENGLAND, F Jul 14-17, 2019 [C]. 2019.